Interaction of tides, groundwater levels and surface moisture on a sandy beach

MSc thesis Earth Surface and Water – Coastal Dynamics and Fluvial Systems

Student: Laura Brakenhoff (3583740)

Supervisor: prof. dr. B.G. Ruessink

Final version: 1st of September, 2015

Universiteit Utrecht

Abstract

Wind-driven (aeolian) sand transport from the beach is of prime importance to coastal dune formation and growth, as well as dune recovery after a severe storm. The amount of aeolian sand transport is not only determined by wind speed, but also by beach surface characteristics, predominantly moisture content. The surface moisture content is determined by processes in the atmosphere (evaporation and precipitation) and in the groundwater (via capillary transport). The groundwater level below the beach is governed mostly by the tide. However, the exact importance of the tide in determining surface moisture content is still unknown. Therefore, the present study aims to find this relation, in order to better understand and predict aeolian sediment transport patterns in the future.

A six-week field campaign was performed at the Sand Motor, near The Hague (NL) in fall 2014. Sea surface elevation was measured with a pressure transducer below the low-water line, while 8 dipwells were deployed to measure groundwater levels in a 80-m long cross-shore array. A Delta T Theta probe was used to measure surface moisture content along the same array. The height of the capillary fringe above the ground water level was estimated, using a grain size of 400µm, to be about 0.2m.

It was found that the tide and the bed profile control the spatial and temporal patterns in surface moisture content. The tidal oscillations in the sea surface propagate into the beach, which makes the water table below the beach oscillate with tidal frequency. The inland water table of the Sand Motor is located 1m above NAP. The slope of the water table is relatively constant, and it is independent of the slope of the beach surface. Therefore, a low beach slope results in an intersection of the water table and the bed surface. This gives a high surface moisture content.

The water table affects the surface moisture content at the Sand Motor when it is within 0.3m below the bed surface. In this case the potential for aeolian sand transport can be reduced, since the surface moisture contents are above 10%. A spring-neap tidal cycle was found in the amount of time throughout the day that this influence was present. During neap tide, the groundwater level was further below the surface, so the capillary fringe could reach the surface for a smaller amount of time. therefore, the potential for aeolian sand transport will be highest during neap tide.

Contents

List of Figures

List of Tables

1. Introduction

On sandy beaches, aeolian sediment transport is of prime importance to coastal dune formation and growth, as well as dune recovery after severe storms. The amount of transport is not only determined by wind speed, but also by surface characteristics like moisture content (in which the surface is defined as the uppermost few layers of grains). Moisture 'glues' the sediment together: the increased adhesion prohibits entrainment by wind, and increases the critical fetch length (Davidson-Arnott and Dawson, 2001). As a consequence, the surface moisture content should be low for aeolian transport to occur. Field experiments have shown that the critical moisture content above which aeolian sediment transport is prohibited, is approximately 4-10% moisture gravimetrically (Wiggs et al., 2004; Davidson-Arnott et al., 2007).

The surface moisture content is determined by processes in the atmosphere (evaporation and precipitation) and in the groundwater (via capillary transport) (Figure 1-1). The groundwater level below the beach is in turn influenced by variations in sea surface elevation (Figure 1-1), of which tide is the most important.

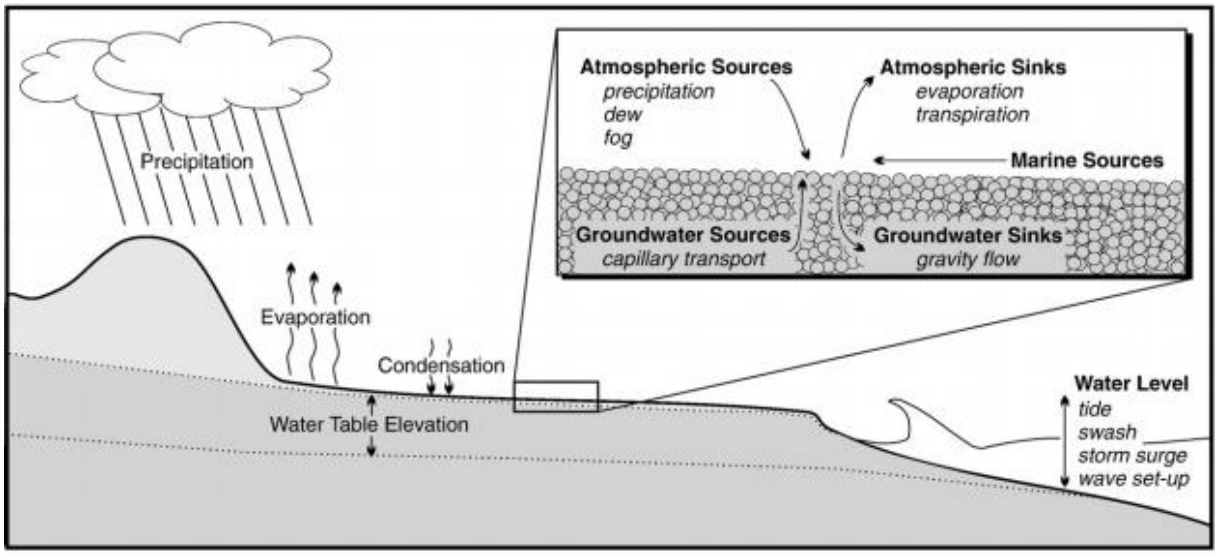

Figure 1-1. The processes that influence the surface moisture content of a sandy beach (Namikas et al., 2010)

Although a lot of work has been done on the propagation of tides through beaches and the effect of water table depth on surface moisture content, only a few studies have explored changes in surface moisture content in association with a change in sea surface elevation due to tides. After several studies (e.g. Darke and Mckenna Neuman, 2008; Oblinger and Anthony, 2008) suggested that tidal elevation and surface moisture content are indeed related, only two studies have focused specifically on this topic. Namikas et al. (2010) measured surface moisture on a sandy beach, but on a very small time (52h) and spatial (20*20m) scale. Due to the short term data set the relative importance of tides and atmospheric parameters could not be determined. Schmutz and Namikas (2013) performed a series of laboratory experiments. A linear tidal signal was imposed upon a sand column, and it was found that tidal oscillations are indeed important in determining surface moisture. However, this experiment has yet to be validated in the field, where the tidal signal is never linear.

In short, the exact importance of tide in determining surface moisture content is unknown. Therefore, in this thesis, the interaction between tides, groundwater levels and surface moisture content is examined by means of a literature study and a field campaign on a wide sandy beach. The field experiment was performed near The Hague, at the Sand Engine.

2. Literature review

2.1 Marine influences on surface moisture content

2.1.1 The effect of tidal variations on groundwater level

Water table oscillations

Beaches can in most cases be seen as unconfined aquifers; groundwater can flow in any direction and the water table can set up itself freely. By definition, the surface of the water table (the groundwater level) is the location where pore water pressure is equal to atmospheric pressure. Below the water table, all pores in the sediment are completely filled with water. Here, pore water pressure is larger than the atmospheric pressure (Horn, 2002).

Oscillations of the beach water table can have several causes: seasonal variations in sea water level (Clarke and Eliot, 1983), barometric pressure variations, wave incidence, rainfall and/or tides (Turner and Nielsen, 1997). However, most studies have focused only on the influence of tides. This is because sandy beaches can be seen as low-pass filters. This is visualized in Figure 2-1: the original tidal period of 12 hours increases to approximately 140 hours high up the beach. This implies that especially low frequency oscillations can propagate inland through the sediment, and short waves are thus filtered (Emery and Gale, 1951; Hegge and Masselink, 1991; Horn, 2002). The filtering is strongest in fine sand, because hydraulic conductivity decreases with grain size (Baird and Horn, 1996). As a consequence, water table oscillations with sea-swell frequency can only be found up to 15m landward of the mean sea level at a beach with a median grain size of 0.35mm and a saturated hydraulic conductivity (K) of 0.077 cm/s (Hegge and Masselink, 1991). A modelling exercise by Li et al. (2000a) resulted in a frequency dampening length of 8m, when K was assumed to be 0.049 cm/s. The filtering of short waves does not only mean that tides will have more effect on the landward water table than sea/swell waves, but also that spring-neap tidal oscillations can propagate up to five times further into the beach sediment than diurnal and semi-diurnal oscillations (Raubenheimer et al., 1999; Li et al., 2000b).

Figure 2-1 also shows that the spectral density (which represents the amount of energy, and is therefore a measure of amplitude) decreases from 200 in the tide to 1.0 high up the beach. This dampening is visible in Figure 2-2 as well: the water table amplitude is about 20 times smaller than the tidal amplitude. The inland amplitude dampening happens exponentially with distance but less dampening takes place when the beach gradient is higher (Mao et al., 2006; Liu et al., 2012). Cartwright (2004) found that the groundwater level fluctuates with semi-diurnal tidal frequency up to 125m landward of the shoreline, at the east coast of Australia (median grain size 0.20-0.25mm, according to Laycock, 1978). Further landward, oscillations were not visible anymore.

Due to the nonlinear filtering by the beach sand, a time lag is established between the tidal elevation and the beach water table elevation (as observed in Figure 2-2 by a shift in time of the maximum water level) (Nielsen, 1990). This time lag increases linearly with distance (Mao et al., 2006), and can be up to 4 hours at the spring high water line (Pollock and Hummon, 1971). The time lag does not depend on the slope of the beach (Liu et al., 2012).

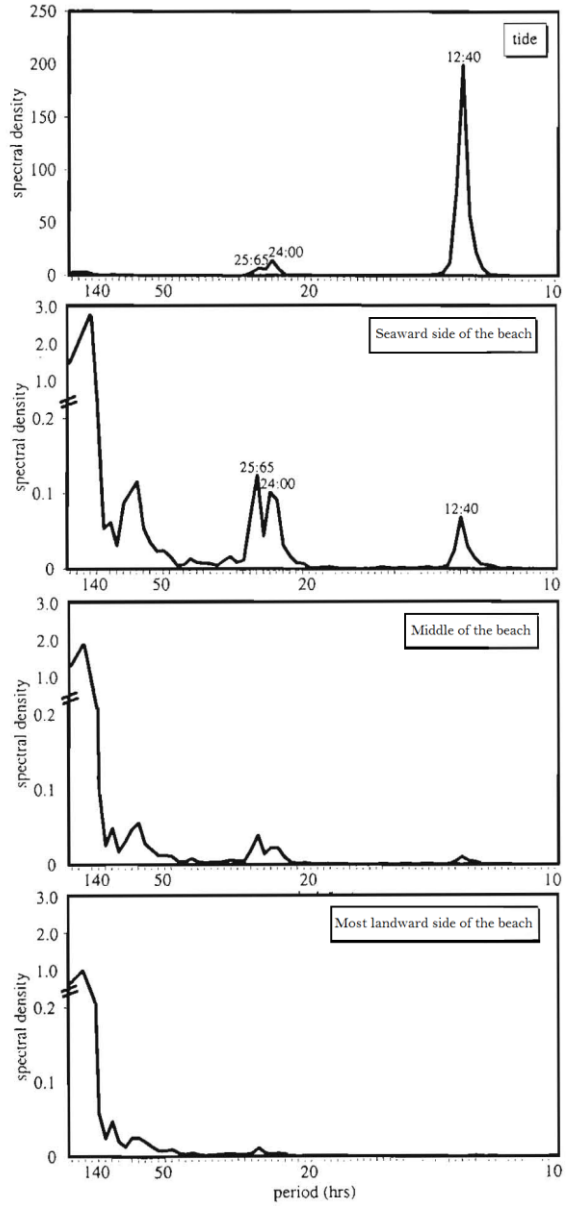

Figure 2-1. Spectral analysis of groundwater oscillations. Most landward side was located 30m from beach face. In landward direction, the amplitude and frequency of the water table oscillation spectrum decrease, so it becomes narrower and is shifted towards lower frequencies (Lewandowski and Zeidler, 1978; Turner et al., 1997). (modified from Turner et al., 1997)

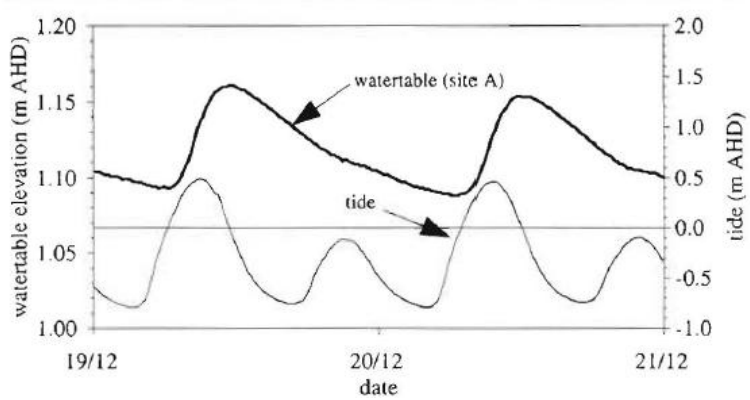

Figure 2-2. Observed differences between variations in the tide and the water table (Turner et al., 1997). Site A is the approximate high water line during spring tide (at the upper beach face). AHD= Australian Height Datum ≈ mean sea level

Overheight

As already visible in Figure 1-1 and Figure 2-2, the water table below the beach surface is not a horizontal continuation of the sea level. Philip (1973) was the first to prove that the water table below the beach is always elevated considerably above mean sea level; he called this the inland overheight. The overheight arises due to several processes.

First of all, infiltration happens vertically when the sea surface elevation is higher than the water table, which makes it governed by gravity. Exfiltration on the other hand, happens when the water table is higher than the sea surface elevation. This is a horizontal process, driven by the local hydraulic gradient. The hydraulic gradient is a weaker force than gravity, so the outflow is slower (Nielsen, 1990; Turner et al., 1996, 1997). This process is enhanced by the fact that at high water, a larger area of the beach is available for water to infiltrate, than there is at low water for the water to drain away again (Horn, 2002).

Earlier studies had used a linear function as representative of the tide to find the water table height below the beach, which they found to be equal to mean sea level. Philip (1973) demonstrated that this assumption was not justified, as tides are represented better by a non-linear sinusoidal function. When this was implemented in the Boussinesq equation (an equation to model unsteady groundwater flow in a homogeneous soil), it was found that the inland water table was in all cases higher than mean sea level. This is because the inland overheight H can be represented as

$$H = \frac{A^2}{4d} \quad \textbf{(1)}$$

in which A is tidal amplitude, and d is aquifer depth (Philip, 1973, rewritten by Nielsen, 1990).

Nevertheless, the overheight as predicted by Equation 1 is always smaller than observed, because Philip (1973) had still used the same main assumption as previous researchers: a vertical beach face. When Nielsen (1990) implemented a sloping surface into the Boussinesq equation, he showed that the slope caused the overheight to increase. The inland overheight is highest for low sloping beaches (Raubenheimer et al., 1999; Ataie-Ashtiani et al., 2001).

The overheight was observed to be on average 1.2m above mean sea level at the east coast of Australia (Turner et al., 1996) and 2m above mean sea level at the west coast of Scotland (Mao et al., 2006). When the beach is subjected to high wave energy, wave run-up can cause the overheight to rise with several extra meters (Nielsen, 1990). Another very important process in the swash zone is the time-averaged component of the short waves; the set-up (Turner et al., 1997). As long as wave action is significant at a coast, the set-up at the shoreline can be in the order of 40% of the offshore root-mean-square wave height (Hanslow and Nielsen, 1993 in: Cartwright, 2004). This means that if waves are important, the overheight will be higher than in environments with tides only. Rainfall and storm waves can also increase the overheight (Turner et al., 1996, 1997). When tides are very high for a relatively short period (for example high tide at spring tide or with a storm surge) the gradient can even reverse, with the water table higher near the coast than more inland (Turner et al., 1996; Ataie-Ashtiani et al., 2001; Abarca et al., 2013). However, if this situation continues, the inland water table rises until a new equilibrium is established (Ataie-Ashtiani et al., 2001).

Coupling, decoupling and asymmetry

The differences between infiltration and exfiltration, which were mentioned above, do not only cause the overheight. They are also the driving factor behind some other processes. The first process that can be observed is decoupling and coupling of the tide and the groundwater level, which is visible in the point where the groundwater departs from the beach (Turner, 1993). When the tide

starts falling, this exit point initially falls at the same rate, so the water table intersects the beach at the sea surface elevation (SSE) of that moment. At a certain point, the exit point cannot keep up with the tidal fall rate anymore, so the water table and the tide are decoupled (Figure 2-3). When the tide rises again, the exit point keeps falling, when it is not reached by the tide. Eventually the exit point is overtopped by the tide, after which the two are coupled again, and rise at the same speed.

The quick infiltration and slow outflow, together with this coupling and decoupling, cause another feature, which can be observed in Figure 2-2: the inland change of the tidal wave shape. The water table rise is forced by the rising tide, but the water table fall is more or less independent. Consequently, while the tidal wave is more or less sinusoidal, the groundwater variation is rather asymmetric, with a steep rise and a slow decline.

Figure 2-3. Definition of the exit point and the seepage face (Cartwright, 2004)

2.1.2 Interactions between groundwater level and surface moisture content

The capillary fringe

The part of the subsurface between the water table and the beach surface is called the unsaturated (or vadose) zone, for the pores in the sediment are not always completely filled with water anymore. The air within the pores makes the pore water pressure less than atmospheric pressure (Horn, 2002). The water in the pores is transported upwards from the water table by capillary action. This is the combined action of the attraction between water molecules (surface tension) and the molecular attraction between water and sediment particles. The surface tension can lift the water into the pore, until the height where the surface tension force is in equilibrium with the weight of the column of water that it is lifting. In this zone, just above the water table, the tension is so high that the pores are completely filled with water. This zone is called the capillary fringe (Figure 2-4) (Turner and Nielsen, 1997; Horn, 2002; Hendriks, 2010). Yet, the pore pressure is still negative, so the capillary fringe is clearly different from the groundwater zone.

It is evident that when the water table or the upper part of the capillary fringe intersects the beach surface, surface moisture content is very high, and aeolian sediment transport is prohibited. If the water table surface drops below the capillary fringe thickness, its influence on surface moisture will diminish and as a result the surface sediment is dry (Figure 2-4) (Cartwright, 2004; Namikas et al., 2010). However, especially in the intertidal area the water table usually lies within 0.1m of the surface (Darke and McKenna Neuman, 2008), so the surface will not become dry very often (Yang and Davidson-Arnott, 2005; Namikas et al., 2010). Yet, it should be noted that the depth of the water

table and the height of the capillary fringe are very dependent on the characteristics of the specific beach.

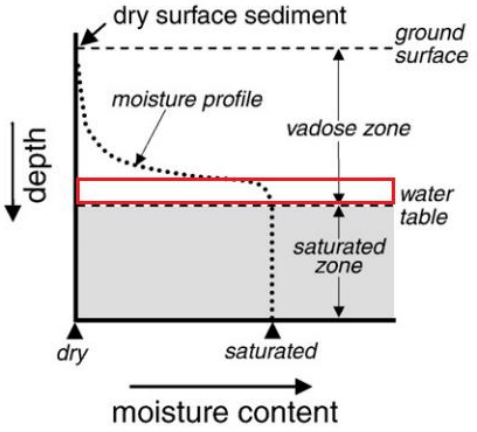

Figure 2-4. Definition of the capillary fringe (red square). In this case, water table depth is larger than the thickness of the capillary fringe, so the surface is dry. (Modified from: Namikas et al., 2010)

The thickness of the capillary fringe might vary in space, because it depends on surface tension and the size of the pores. A medium with small grain size and thus small pores (like clay) will have a higher capillary rise above the water table than a medium with larger pores (like sand or gravel) (Ataie-Ashtiani et al., 2001; Cartwright, 2004; Hendriks, 2010). The thickness of the capillary fringe H_c can be estimated as:

$$H_c = \frac{10\gamma}{\rho g D} \quad \textbf{(2)}$$

where γ is the surface tension of the water, ρ is the water density, g is gravitational acceleration and D is the mean particle diameter (Turner and Nielsen, 1997; Darke and McKenna Neuman, 2008). Theoretically, this leads to a capillary rise as given in Figure 2-5, which shows that water movement through the capillary fringe is especially important on medium- to fine sand beaches (D<0.3mm) (Turner and Nielsen, 1997; Darke and McKenna Neuman, 2008). Gillham (1984) found similar values: the capillary fringe thickness ranges from 0.01m (in very coarse sand) to 1m (in very fine sand). More recent studies confirmed this: for fine to medium sand a capillary fringe thickness of 0.3m (Atherton et al., 2001) to 0.5m (Yang and Davidson-Arnott, 2005; Darke and McKenna Neuman, 2008) was found.

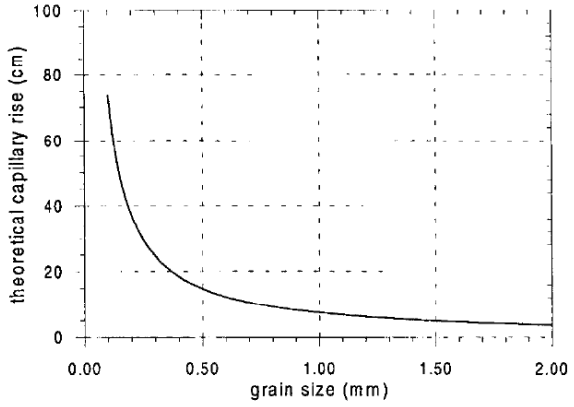

Figure 2-5. Theoretical capillary rise (Turner and Nielsen, 1997)

When the moisture content is lower than 8%, the adhesion of the water does not depend on the grain size, since the representative contact angle of the particle does not depend on its diameter either (Figure 2-6) (Hotta et al., 1984). At higher moisture contents, the adhesion becomes dependent on gravity, until the grains become too large and stable water bridges cannot be formed anymore. Therefore, on coarse sand beaches the water drains to the water table instead of remaining in the capillary fringe. On top of that, larger grain size gives larger hydraulic conductivity, which makes drainage even easier (Hendriks, 2010).

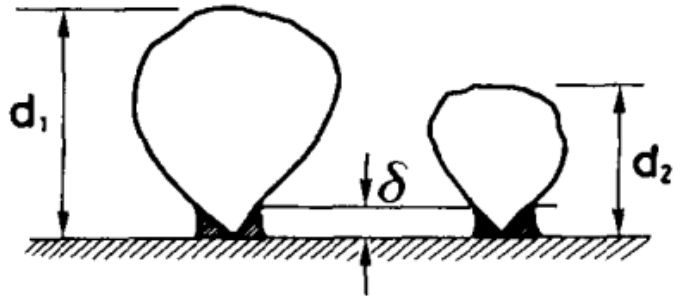

Figure 2-6. Two grains, with d1>d2, but δ (thickness of the water bridge) is the same (Hotta et al., 1984).

Next to grain size, hydraulic conductivity also depends on moisture content. Air within pores can block the flow, so water can flow faster through the capillary fringe when moisture content is higher (Baird and Horn, 1996). The associated increase in hydraulic conductivity ranges over several orders of magnitude: from $3 \cdot 10^{-7}$ m/s for dry sand to $5.5 \cdot 10^{-4}$ m/s when the sand is saturated (Janssen et al., 2004). This can lead to a time lag between the maximum height of the water table and the maximum surface moisture content. In space, the impact of the time lag increases with water table depth, so on a beach this will be in the onshore direction. When the water table is 60cm below the surface, the time lag between the high water level of the groundwater and the maximum surface moisture content can be 2 hours, while the time lag between low water and the minimum moisture content can be even twice as large (Schmutz and Namikas, 2013).

The capillary fringe also affects movements of the water table, but this is most important for the water table oscillations at high frequencies (Li et al., 1997; Li et al., 2000a; Cartwright et al., 2005). However, as stated before, this is only important in the swash zone. At a semi-diurnal tidal frequency (~12h), the capillary fringe has little effect on dispersion of the water table wave (Li et al., 1997; Cartwright, 2004).

Hysteresis

As stated before, the time lag between groundwater level and surface moisture content is larger at falling tide than at rising tide. This is due to a process called hysteresis, which means that the drying and wetting of the soil happen in different ways (Figure 2-7). At falling tide, the soil moisture content initially remains the same. Only when the suction reaches a certain high value, the water from the soil column suddenly drains to the water table. Equally, when the suction decreases again (at wetting), the moisture content first remains low, until a point is reached where the pores are suddenly filled with water when the capillary fringe reaches the surface (Schmutz and Namikas, 2013). This process is called the 'ink bottle effect' (Figure 2-7. The ink bottle effect: hysteresis (www2.nau.edu)Figure 2-7). The importance of hysteresis increases with decreasing grain size, because these sediments have higher suction values (Yang et al., 2004).

Hysteresis and the ink bottle effect result in a higher moisture content at the same suction in a drying soil (during ebb) than in a wetting soil (during flood) (Khaled et al., 2011; Schmutz and Namikas, 2013). Thus, the surface moisture content is dependent on its own history.

The capillary fringe thickness oscillates on a tidal timescale, which is also due to hysteresis effects. When the water table is falling, surface tension increases, so the top of the fringe does not lower as fast as the water table, and the capillary fringe thickens (Turner and Nielsen, 1997). Thus, the upper limit of the capillary fringe oscillates much less, and its maximum elevation is observed later in time than the maximum elevation of the water table (Cartwright, 2004).

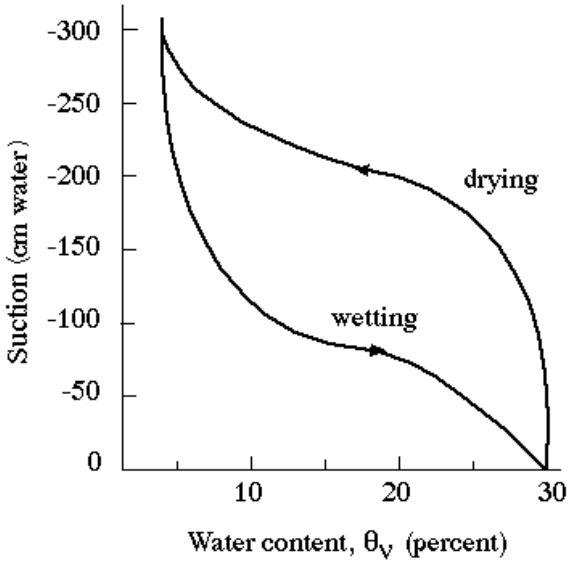

Figure 2-7. The ink bottle effect: hysteresis (www2.nau.edu)

2.2 Atmospheric influences on surface moisture content

Beach surface moisture dynamics have now been explained by tidal dynamics, which cause oscillations in the beach groundwater level and thickness of the capillary fringe. However, there are several more parameters affecting surface moisture content, as given in Figure 1-1-1. This chapter examines the atmospheric sources and sinks: precipitation and evaporation.

2.2.1 The effects of precipitation on surface moisture content

The Lisse effect

It is evident that directly after a rainfall event, the measured surface moisture content is not at all related to the depth of the water table or the height of the capillary fringe (Figure 2-8). Apart from its influence on surface moisture content, precipitation also affects the groundwater level in several ways. The most common process is that precipitation infiltrates into the soil and thereby recharges the groundwater. It should be noted here that this is only important in the case of an intense precipitation event, since most events in the Netherlands only consist of a few millimetres of rain, which will not significantly affect the groundwater level.

The second phenomenon caused by precipitation is the Lisse effect, which indicates a disproportional high rise in the capillary fringe after a severe rain event. This happens because the precipitation 'seals' the surface, so air cannot flow in or out anymore. As the precipitation infiltrates, the air trapped within the unsaturated zone is compressed, which increases the air pressure in the pores. The water level below the infiltration location (and therefore also the capillary fringe) rises to compensate for this increase. The magnitude of the rise can be in the order of several decimetres (Miyazaki et al., 2012). This rise happens very fast, but the return to its original state can take several days. The Lisse effect occurs when the water table is between 0.6 and 1m below the sand surface (Guo et al., 2008; Miyazaki et al., 2012).

The Lisse effect is a clear example of precipitation influencing both groundwater level and surface moisture content. The observed variations in this case have nothing to do with tidal oscillations, but especially the groundwater level is affected on a timescale larger than that of the tide.

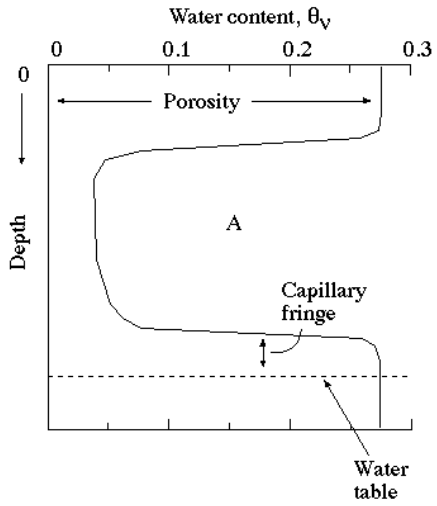

Figure 2-8. Moisture profile after rainfall (www2.nau.edu).

The reverse Wieringermeer effect

Another process in which precipitation influences both the water level and the surface moisture content is the reverse Wieringermeer effect. This effect occurs when the upper limit of the capillary

fringe is almost intersecting the beach surface. A small amount of precipitation can change the pressure from lower than atmospheric to higher than atmospheric (for it relieves the capillary tension), and may thus fill all pores that still contained air. This leads to a very rapid rise in water and capillary fringe level (Figure 2-9) (Gillham, 1984; Miyazaki et al., 2012). For example, in a laboratory experiment Gillham (1984) found a water table rise of 30cm in 25min when only 3mm of water was added to the surface. Contrary to the Lisse effect, the reverse Wieringermeer effect is characterized by an equally sharp rise and decline in water level.

A similar process was observed by Turner and Nielsen (1997) and Cartwright (2004). When tidal elevation and was low, the location of the exit point remained in the upper part of the intertidal zone. This happened because the water table was close to the surface, so the capillary fringe and the beach surface were intersecting. Only a small amount of rain (in the order of a grain diameter) could bring the water table to the surface and create an exit point (Turner and Nielsen, 1997).

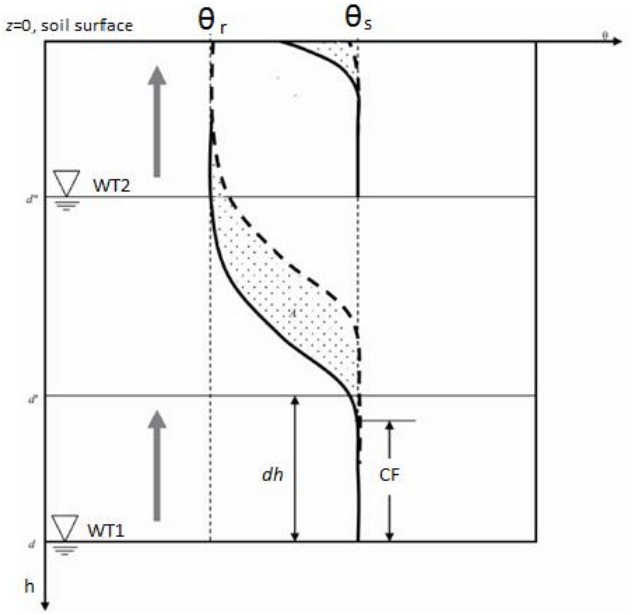

Figure 2-9. Moisture profiles above a deep (WT1) and a shallow (WT2) rising water table. The dotted area gives the amount of added water, CF=capillary fringe, θr=residual moisture content, θs=saturated moisture content. At WT2, the dotted area is smaller than at WT1, so less water has to be added to obtain a rise in surface moisture content (Khaled et al., 2011).

2.2.2 The effect of evaporation on surface moisture content

Evaporation is (together with the water table) the basis of the capillary force. When water is evaporated at the surface, the matric potential difference (suction) between the water table and the surface increases, which leads to water moving upward through the capillary fringe. For shallow water tables, this process can be very fast, and is referred to as the Wieringermeer effect. It works the same as the reverse Wieringermeer effect that is described above.

Measuring evaporation is very time-consuming, and it is hard to get reliable results (Hendriks, 2010). With the knowledge that evaporation is caused by either the air temperature, solar radiation or wind, some formulas have been established, so it is now possible to calculate the amount of evaporation. Usually, the evaporation from a reference crop is calculated: a densely vegetated healthy grass field of 0.1m high. To get the potential evaporation, reference crop evaporation should be multiplied by a crop factor f. For unvegetated sand, f≈0.75 (Pastoors, 1992) - 0.9 (Roelsma et al., 2008). The most common formula to calculate reference crop evaporation E_{rc} in mm/day is the Penman-Monteith equation:

$$E_{rc} = 0.408 \cdot \frac{\Delta R_n + \frac{105.028(e_s - e_a)}{r_a}}{\Delta + 0.067\left(1 + \frac{r_s}{r_a}\right)} \quad \textbf{(3)}$$

In this formula,

$$\Delta = \frac{4098 \cdot 0.6108 \cdot e^{\frac{17.27T}{237.3+T}}}{(237.3 + T)^2} \quad \textbf{(4)}$$

In equation (3), Δ = the gradient of the saturation pressure curve,(kPa/^{o}C),

R_n = the net radiation at the earth's surface (MJ/m^2/day),

e_s = the saturation vapour pressure (kPa),

e_a = the actual vapour pressure (kPa),

r_a = aerodynamic resistance (s/m) and

r_s = surface resistance (s/m).

In equation (4), T denotes temperature (^{o}C).

The resistances are specific for a given soil and vegetation type. They cannot be measured, but have to be estimated. All other variables can be calculated from the net radiation R_n, air temperature and relative humidity, which are measurable. The Penman-Monteith equation is the most commonly used evaporation equation, and is applicable everywhere on earth. When only a small area is studied, so climate and incoming radiation can be considered constant in space, the Penman-Monteith equation can be simplified. For the Netherlands, it is reduced to the Makkink equation (Hendriks, 2010):

$$E_{MK} = C_{MK} \frac{1000}{\rho\lambda} \frac{\Delta}{\Delta + \gamma} S_t \quad \textbf{(5)}$$

In this formula, C_{MK} = Makkink constant = 0.65 for a humid climate like the Netherlands (-)

ρ = water density ≈ 1000 (kg/m^3)

λ = latent heat of vaporization ≈ 2.45 (MJ/kg)

γ = psychometric constant ≈ 0.067 (kPa/^{o}C)

S_t = incoming shortwave radiation (MJ/m^2/day)

C_{MK} contains all values that were present in the Penman-Monteith equation, but are not visible in the Makkink equation. All other variables in the Makkink equation are only dependent on air temperature and incoming shortwave radiation S_t, which are (relatively) easy to measure.

The evaporation that results from Equation 5 is given in mm/day, which is too long to compare with the surface moisture variations on a tidal time scale. To find the evaporation in mm/h, the mean temperature per hour should be used and the incoming shortwave radiation should be given in MJ/m^2/h (Hendriks, 2014, personal communication). It is not known whether C_{MK} is still correct in this case, but it will at least give a representative estimation.

Evaporation functions as a positive feedback: when surface moisture content is high, a lot of water is available, so a lot of evaporation takes place. This leads to a lower surface moisture content, with less water available, so increasingly less evaporation will take place (Schmutz, 2014). Spatially, this means that the evaporation rate decreases in landward direction. Therefore, only the actual evaporation near the swash zone will resemble the potential evaporation that was given by E_{MK} the best. Further landward, the actual evaporation is always lower than E_{MK} (Schmutz, 2014).

3. Main objective and research questions

3.1 Main objective

From the literature survey that is presented here, it can be deduced that the propagation of the tide through the beach is largely known. Previous research has also found an effect of the groundwater level and meteorological parameters like precipitation and evaporation on the surface moisture content. All these factors should be considered at the same time, if the full complexity of the surface moisture content dynamics is ever to be understood. Therefore, the objective of the present study is to get a better understanding of the variability of surface moisture content in time and space. The main goal is to find how far onto the beach tide and surface moisture content are related. With this knowledge, the spatial and temporal patterns in aeolian transport might be understood better in the future.

3.2 Research questions

The main question for this study is: *What is the relation between tidal oscillations in the water table and variations in surface moisture content on a sandy beach?* To answer the main question, sub questions are defined, which are divided into questions about the tide (1) and questions about surface moisture (2).

Sub questions:

1. What is the effect of tidal oscillations on the groundwater table of the beach?

1A. What changes are experienced by the tidal wave when it propagates through the beach?

1B. How far into the beach is the water table high enough for the capillary fringe to bring water to the surface?

2. To what extent do tidal oscillations of the groundwater table determine the surface moisture content of the beach?

2A. Until what height above the high water line is surface moisture variable with tidal frequency?

2B. What is the relative importance of the tide in determining surface moisture content?

3.3 Hypotheses

Even though the exact subject of the present study has not been studied before, some hypotheses could already be made using the literature presented in Chapter 2. For example, the tidal wave will be damped exponentially while it travels through the beach. Its asymmetry will increase, and a time lag will arise between the tidal elevation and the groundwater level.

It is a well-known phenomenon that the differences between infiltration and exfiltration cause the inland water table to rise above mean sea level. It is therefore highly likely that this is also found in the present study. The overheight is expected to hold surface moisture contents high at low tide, especially within the intertidal area of the beach.

Another variable that might be of importance is the beach slope. It is expected that with a higher slope, the groundwater level at a certain distance inland is lower than with a lower slope, as found earlier by Raubenheimer et al. (1999) and Ataie-Ashtiani et al. (2001). Therefore it will take more time for the capillary fringe to reach the surface, so the surface moisture content will be lower.

It is expected that precipitation will increase the surface moisture content, or keep it at the same level when drying was taking place before the precipitation. The opposite goes for evaporation: this will most probably decrease the surface moisture content, or keep it at the same level when wetting was taking place.

4. Methods

4.1 Description of the study site

To find answers to the research questions, a field experiment was carried out at the Sand Motor (also known as Sand Engine). The Sand Motor is located at the south-western coast of the Netherlands, near The Hague (Figure 4-1). It is a mega nourishment created in 2011, with 21.5 million m^3 of sand deposited on the shoreface. The sand was taken from approximately 10km offshore (Stive et al., 2013). Natural processes, like wind and waves, are supposed to spread this sediment along the coast, thereby increasing coastal safety in the Netherlands. Currently the Sand Motor is still a constantly changing environment.

The study site was located on the southern part of the Sand Motor, because this is morphologically the most stable part. At this location, the intertidal area has a slope of 1:40 and the distance from the water line to the dunes is approximately 500m. The measurement campaign took place from the 15th of September to the 23rd of October, 2014.

Figure 4-1. Location of the Sand Motor in the Netherlands. The red dot marks the study site. (Modified from: www.coastalresearch.nl)

4.2 Field methods

4.2.1 Groundwater level

Groundwater levels were determined with 8 dipwells in a cross-shore array from the mean low water line to above the spring high water line. These dipwells consisted of steel tubes of 2-4m in length and 0.05m in diameter, with a perforated lower end of approximately 1m. In the steel tube a PVC pipe was inserted, with a filter of 50µm at the lower end, to prevent any entering of sand. From September 15 to September 29, groundwater levels were determined manually every 30 minutes. This was done with a hollow weight, which was attached to several meters of measurement tape. This weight was lowered into the dipwell, and gave a sound when it reached the water table. The water table depth relative to the top of the dipwell could then be read from the measurement tape. The height of the top of the dipwell relative to Dutch Ordnance Datum (NAP) was determined with

an RTK GPS device (Appendix A.1). These and all other coordinates determined during the field campaign were measured in the RD2008 coordinate system.

From October 11 to October 23, Keller 3.1 sensors were deployed in the dipwells. The Keller sensors measure the total of the air and water pressure (in mBar), so an extra sensor was deployed on land to measure air pressure. The measurement frequency of the sensors was set to once every 10 minutes, to exclude the recording of any possible sea-swell waves that might intrude into the beach. The locations (x, y and z coordinates) of the beach surface next to the dipwells were determined with an RTK GPS device every day (see Appendix A.2). On top of that, the height from the bed to the top of the dipwell was measured with measuring tape every day. The length of the rope and sensor was measured twice: before and after the field campaign. The locations of the dipwells and the sensors during this period are given in Figure 4-2. GW1-GW5 are permanently below the high water level. GW6 is only below the high water level during spring tide, and GW7 and GW8 are permanently above the high water level.

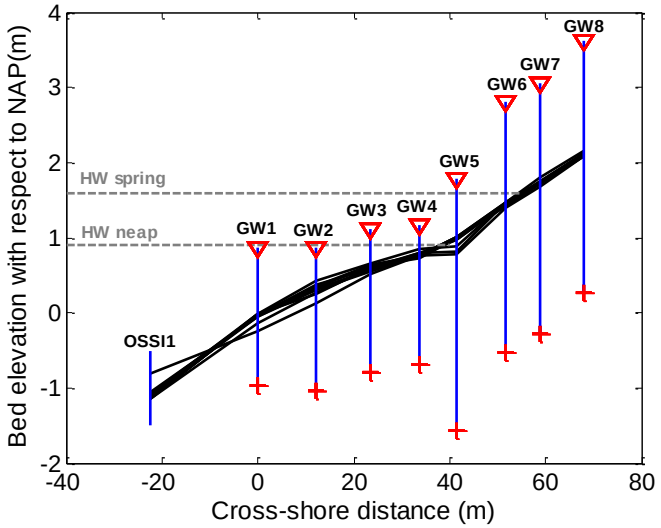

Figure 4-2. Placement of the dipwells and the pressure transducer, with all bed profiles from 11-23 October. Crosses mark the sensors. High water levels during spring and neap tide are displayed in grey. Cross-shore distance is with respect to GW1, positive onshore.

4.2.2 Surface moisture content

Surface moisture content was measured with a Delta T Theta probe, along an array parallel to the dipwells. The probe measures the dielectric constant (ε) of the sediment (Gaskin and Miller, 1996; Yang and Davidson-Arnott, 2005). ε depends on both sediment properties and moisture content, so if the sediment is relatively uniform, the output of the probe can be used to derive the surface moisture content. The probe contains four stainless steel rods that are inserted into the sediment, where the probe generates and transmits a 100MHz signal. The difference in impedance between the rods and the soil results in a reflection of this signal, given as a voltage (Gaskin and Miller, 1996). Usually, the rods are 6cm long, but this is not representative of the actual surface. Therefore, the rods were shortened to 2cm.

Measurements were done every 5-30 minutes, depending on the length of the array that was above the water surface and could thus be sampled. Five measurements were done per location, to account for variability in the sediment and uncertainties in the probe output. Measuring was done for 6-8 hours a day, and during different parts of the tidal cycle on different days.

The x, y and z coordinates of each sample location were determined with an RTK GPS device. Due to technical issues, a new probe was used from the 13th of October. Gravimetric samples were taken

on several days for calibration of the probes, since the salt content of the water might change during a spring-neap cycle.

4.2.3 Tides and waves

Wave height was recorded by a buoy 800m offshore of the study area. The offshore tidal elevation was obtained by linearly interpolating between the tidal elevation at a station near Scheveningen and a station near Hoek van Holland. The study area is located in between these two stations.

The nearshore tidal elevation was derived from a pressure transducer (OSSI1), which was installed 22.5m seaward from GW1 (Figure 4-2, see Appendix A.3 for coordinates). The bed level at this location was variable, but on average OSSI1 was located at -1m NAP, which is below the low water line. The pressure transducer measured the pressure above it with 5Hz. To be able to translate the pressure signal to water level later on, the coordinates with respect to NAP and the height of the instrument above the bed were measured as often as possible. The pressure transducer could not be reached every day, since it was in quite deep water.

4.2.4 Other

For a study of S. Huizer (Utrecht University), a weather station was deployed on the Sand Motor, to gain information about the exact weather conditions at the study site. The weather station measured air pressure, air temperature, precipitation, relative humidity, solar radiation, wind direction and wind velocity, all once per minute. These variables may affect the surface moisture content through precipitation or evaporation.

For the same study, the sediment composition of the Sand Motor was determined through boreholes, and dipwells were deployed across the entire Sand Motor. These dipwells were deployed in couples: at each location one of the dipwells had a filter at 2-10m below the bed, and the other had a filter of 16-20m below the bed. One pair of dipwells was deployed 200m landward of the present measurement array (that was shown in Figure 4-2, see Appendix A.3), and could thus be used to gain additional information on dampening and inland overheight.

4.3 Boundary conditions and data selection

4.3.1 Hydrodynamics

The hydrodynamic boundary conditions during the measurement period are given in Figure 4-3. The tidal signal at the sand Motor is semi-diurnal and quite asymmetric: the water level rises relatively fast, but falls more slowly. Low tide can remain for several hours. The tidal range varies from 1m during neap tide to 2.4m during spring tide. Neap tide occurred around the 19th of September and around the 5th and 19th of October. Spring tide occurred around the 26th of September and the 12th of October. OSSI1 was permanently submerged during the measurement period, so this nearshore tidal elevation could be used for the analysis of the effect of the tide on the groundwater level.

The tidal elevation during the period that the Keller sensors were employed (October 11-23) is representative for the tidal elevation of the entire measurement period. This period also contains an entire cycle from spring to neap tide. On top of that, the Keller sensors can determine the groundwater level more precisely than the manual measurements, and they measure continuously. Therefore, only these data are used in the analysis of the groundwater levels within the beach.

To find the influence of the oscillating water table on the capillary fringe, two days are selected: the 11th and the 18th of October. The 11th of October (spring tide) was a day with calm weather. There was nearly no wind (mean wind speed 4m/s), so wave setup could not have a significant

influence on the groundwater profile. On the 18th of October (neap tide) mean wind speed was approximately 9m/s, but the wind came from the south, so wave set-up is not expected to be important.

Most of the time during the field campaign, wave height was relatively low: the average Hm0 was 0.65m. Yet, Figure 4-3 also shows that a severe storm took place at the 21st of October. During this storm, the offshore wave height increased to almost 5m, and the sea surface elevation was nearly 3m +NAP due to a high surge in combination with high tide. Two smaller storms occurred on the 21st of September and the night before the 5th of October, however these storms are mainly characterised by an increased wave height and not so much by a raised water level.

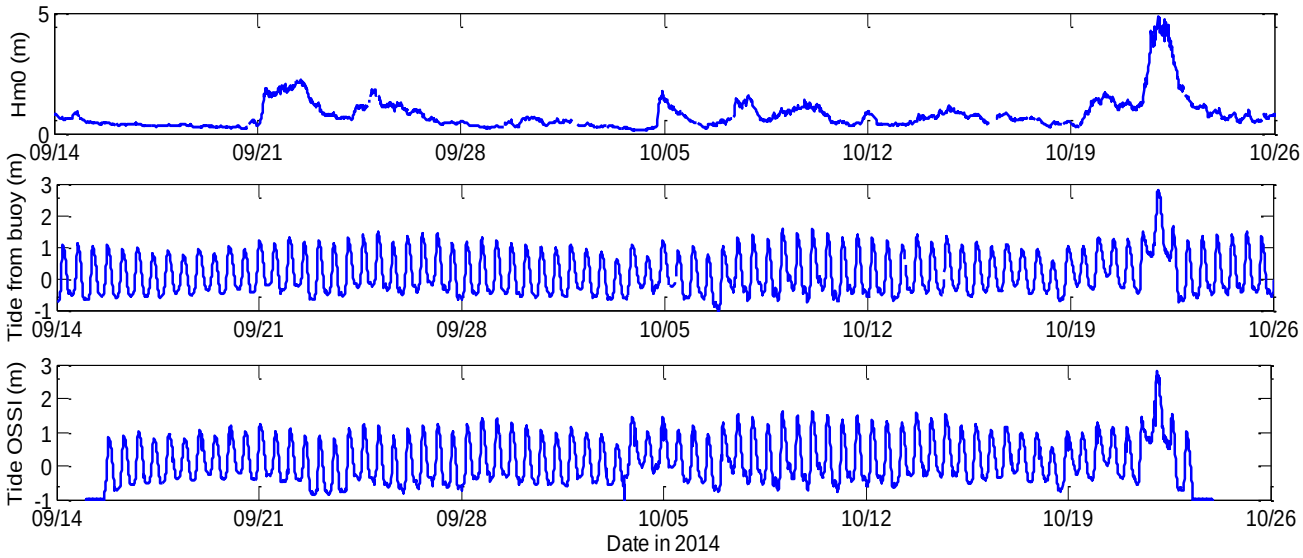

Figure 4-3. Hydrodynamic boundary conditions during the entire measurement period

4.3.2 Meteorology

The differences between storm and non-storm conditions are also visible in the time series of evaporation and precipitation (Figure 4-4). The evaporation shows a clear daily cycle, since it depends on solar radiation and temperature. It is a peaked signal, since the solar radiation immediately decreases when for example a cloud passes by. On days with rain (so more clouds) the amount of evaporation is clearly lower than on days without rain. This happens for example on October 14 and 21.

The storm at October 21 has the most distinct precipitation curve: the amount of precipitation per hour is clearly building up in the beginning of the storm, and decreases after the peak of the storm. The other precipitation events during the measurement period are shorter and more randomly distributed concerning the amounts of precipitation during the event. The small storm in the night before October 5 is characterised by a short, but very intense precipitation event, and during the storm on September 21 hardly any precipitation was measured.

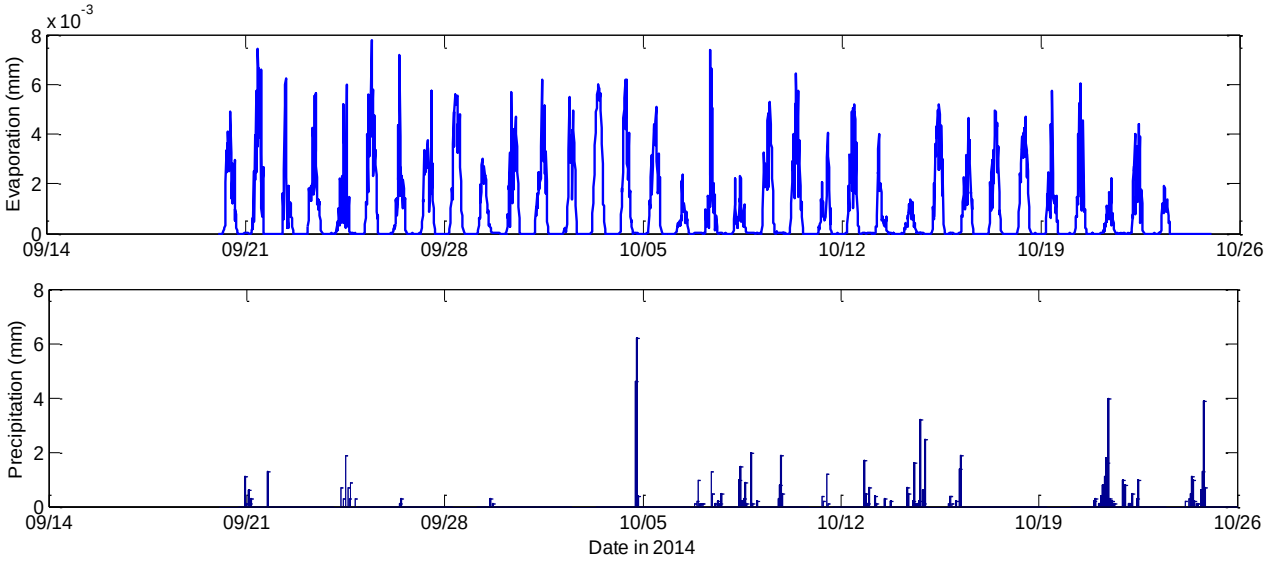

Figure 4-4. Evaporation (from S. Huizer, Utrecht University) and precipitation (data source: KNMI) during the field campaign

All days during the field campaign with rain and surface moisture measurements are given in Table 4-1. The relation between precipitation and surface moisture can only be determined if the precipitation fell during or just before the measurements. This is not always the case, so only the red coloured days are eligible for further analysis. It is further observed that the measurements on September 24 and 29 were done during only 2 hours. Considering the fact that the precipitation data are given in mm/h, this is too short to find a reliable relation. Therefore October 11, 13 and 16 are selected for detailed analysis of the effect of precipitation.

Table 4-1. Correspondence of measuring time and precipitation time during the field campaign

Day	Measurement Time (MET)	Rain Time (MET)
20-09	7:00-12:00	23:00-0:00
21-09	14:30-16:30	2:00-5:00, 18:00-19:00
24-09	12:00-14:00	8:00-9:00, 10:00-11:00, 12:00-13:00, 14:00-17:00, 20:00-21:00
29-09	14:00-16:00	15:00-16:00, 17:00-18:00
04-10	11:00-15:30	18:00-21:00
11-10	10:30-16:00	8:00-10:00, 12:00-14:00
12-10	7:30-15:30	20:00-0:00
13-10	12:00-17:15	5:00-7:00, 13:00-14:00, 18:00-19:00
15-10	7:45-13:30	19:00-23:00
16-10	8:00-14:00	5:00-7:00
20-10	9:00-13:00	23:00-0:00

4.3.3 Morphology

On a large scale, the southern part of the Sand Motor was morphologically stable during the measurement campaign. However, the bed surface elevation of the intertidal area at the measurement location was found to be very dynamic (Figure 4-5). During the first four weeks, an intertidal bar was present. The figure shows that the bar appeared and disappeared twice. In the first two weeks, the bar migrated approximately 10m inland, but between October 2 and 9, the bar

migrated some 20m in landward direction. After October 9, the bar disappeared and the profile remained more or less straight until the end of the campaign (see also Figure 4-2).

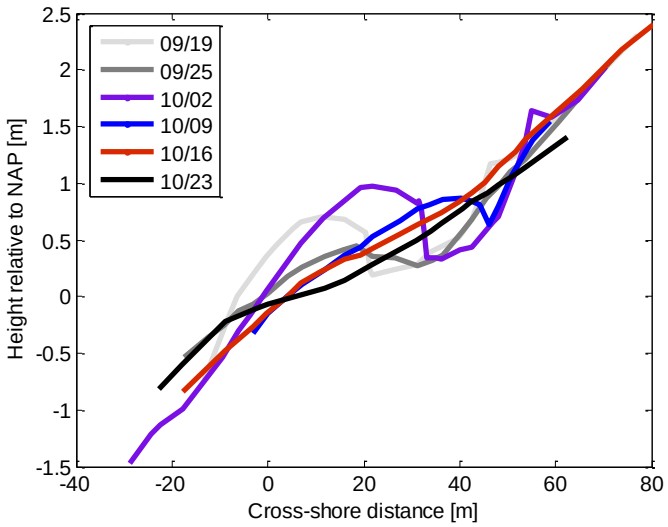

Figure 4-5. Morphological development per week of the measurement area during the field campaign

4.3 Data processing

Both before and after the field campaign, the Keller sensors were tested in the lab, and their offsets were determined (Appendix A.2). This was done by exposing the sensors to a series of known air pressures, and compare these pressures to the sensor outputs. Before the field campaign, all sensors worked well, but the test after the field campaign showed a 'drifting' output of the sensor that was deployed in GW2. This means that the sensor was broken either during or after the field campaign. When the offset was used that was found beforehand, the data of GW2 are in line with those of GW1 and GW3. Therefore, the data of GW2 are not discarded, but conclusions should still be drawn with caution.

The groundwater level h as measured by the Keller sensors was calculated with

$$h = \frac{p * 100}{\rho g} \qquad \textbf{(6)}$$

Water pressure p is given by the calibrated pressure signal from inside the dipwell (air+water pressure) minus the air pressure. It is multiplied by 100 to transform the mBar to Pa. g is gravitational acceleration (9.81 kgm/s^2), and ρ is seawater density, which equals 1025 kg/m^3.

The groundwater level h that is calculated with Equation 6 is actually the water height above the sensor. To convert this to the water level relative to NAP, the height of the sensor with respect to NAP should be added. This height is calculated by taking the bed level, adding the height of the tube from bed to cap, and then subtracting the length of the rope and the sensor from it. The water level from the manual measurements was calculated by subtracting the water depth from the actual height of the top of the dipwell.

Since the sensors measure continuously, whereas the manual measurements could only be done for a limited amount of time per day, most of the data analysis took place using the sensor data. The manually measured waterlevel was converted to a water level relative to NAP by subtracting the water depth from the height of the top of the dipwell.

The bed level at the location of the pressure transducer (OSSI1) for every day was linearly interpolated from the available data. The pressure was converted to a water level above the sensor with the same formula as above. Then, the bed level was subtracted from this, to derive the water

level relative to NAP. Since the measurement frequency was 5Hz, sea-swell and infragravity waves were also measured. These waves were filtered out of the data with a frequency filter. The frequency boundaries at 0 and 0.002Hz reveal the tidal signal.

The high and low water levels for each tide per dipwell were calculated as the maximum and minimum water level per 12-hour period. This was done to ensure that each tide would only be assigned one value for high and low water, since the water level would sometimes also rise and fall during low tide (Figure 4-3).

Two calibration curves were made for the Delta T theta probes, because two different probes were used. The sediment samples that were taken in the field were weighed, oven-dried, and weighed again, to derive the gravimetric moisture content. The calibration curves are obtained by plotting this moisture content against the accompanying probe output (Figure 5-3). In the first calibration curve, data from two days were combined, since they were overlapping, and within each other's 95% confidence bands. R^2 was very high in the linear regression line, so this was used.

For the other probe, the results were clearly not linear. Therefore, a third order calibration curve was made. Using the calibration curves, the probe output was converted to moisture content. Standard errors were calculated with

$$\sqrt{\frac{1}{N-2}\sum_{i=1}^{N}(w_{measured} - w_{predicted})^2} \qquad \textbf{(7)}$$

In this formula, w denotes the surface moisture content and N is the amount of samples. The standard errors are 1.58% moisture for the linear curve and 1.18% moisture for the polynomial fit. These values are both lower than the error of 2% moisture for the 2cm probe used by Schmutz and Namikas (2011).

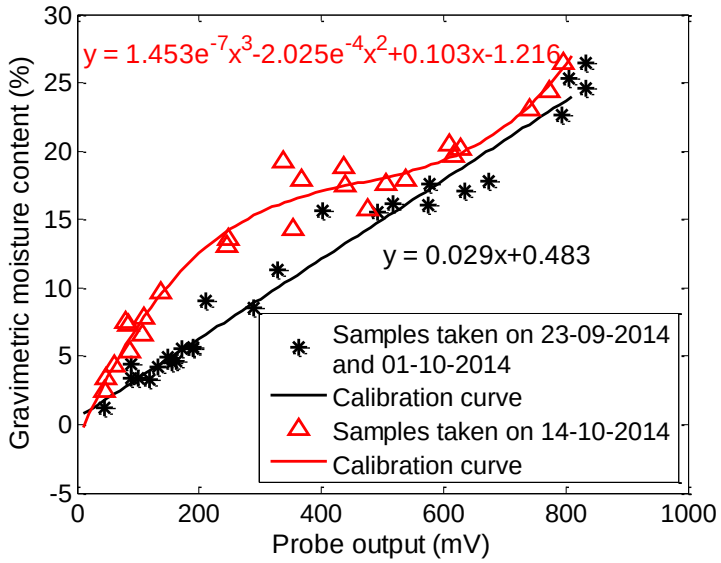

Figure 4-6. Calibration curves of the 2cm probe. The black line has an r^2 of 0.96, and the red line has an r^2 of 0.97.

The precipitation data of the study of S. Huizer were added to derive a precipitation in mm/day. These values were compared to those of the Royal Dutch Institute of Meteorology (KNMI), from the weather station of Hoek van Holland. This station is located approximately 6km to the southwest of the study site, so no large differences should be visible between the two data sets. However, the weather station of the Sand Motor showed significant anomalies, of sometimes 20-30mm per day. Therefore it was decided to use the (hourly) data of the KNMI.

To calculate the amount of evaporation, the measured temperature and solar radiation per minute were inserted in Equations (4) and (5). This resulted in evaporation values with a unit of mm/min. The daily evaporation that was derived by cumulating over a day was the same as the evaporation in mm/day as given at the near-by KNMI station. The evaporation could thus be given in mm/min.

4.4 Data analysis

The tidal range in both the water table and the sea surface elevation were calculated by taking a high water level and subtract the previous low water level. The tidal amplitude is given as the tidal range divided by 2. For this calculation, the storm data were omitted, in order to gain insight into the characteristic amplitude decay over distance at the Sand Motor.

Time lags were calculated by subtracting the time of occurrence of a high water in GW1 from the time of occurrence of the same high water in each following dipwell. High water was used because the peaks were easier to determine than the low water peaks. The calculations of the time lags were done with the data from the entire deployment period of the sensors, to be able to find the evolution of the time lag throughout the spring-neap tidal cycle.

The asymmetry of the tidal and groundwater waves was determined using the method of De Groot (2002), where the asymmetry A was defined as the time from high to low water divided by the duration between the two high waters:

$$A = \frac{t_2 - t_1}{t_3 - t_1} \quad \textbf{(8)}$$

This formula compares the observed wave to a perfect sine, and can have a value between zero and unity. In a sinusoidal wave, the time from high to low water is equal to the time from low to high water, which results in A=0.5. As already explained in Chapter 2.1, when a wave travels through the beach in landward direction, the rising tide remains approximately equally fast, while the falling tide duration increases (see also Figure 4-7). This means that the time from high to low water (t_2-t_1) increases, whereas the tidal period (t_3-t_1) remains the same. Therefore, A will increase. Ultimately, the low tide and the following high tide can almost coincide, causing A to approach 1. This is also observed in the present data set: all values of A are between 0.5 and unity.

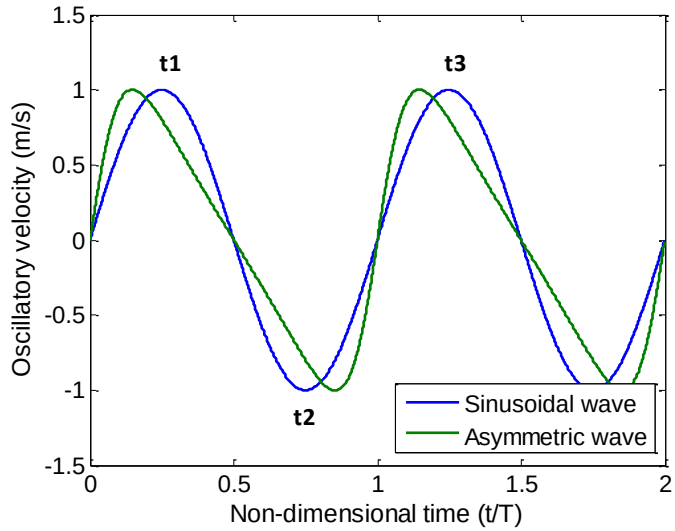

Figure 4-7. Difference between sinusoidal and asymmetric wave shape and definition of asymmetry

The maximum thickness of the capillary fringe H_c was estimated using Equation (2). In the case of the Sand Motor, γ is assumed to be 72.8 mN per meter at 20°C (Hendriks, 2010), ρ equals 1025 kg/m^3, and g equals 9.81 kgm/s^2. Three sediment samples from the gravimetric analysis were sieved to determine their median particle diameter. Sample 2.6 was taken some 30m south of GW1, sample 3.5 was taken 20m more to the south of sample 2.6, and sample 4.3 was taken at 30m south of gw3. Their coordinates, median diameters, and according theoretical capillary fringe thicknesses are given in Table 4-2:

Table 4-2. Grain size samples and according theoretical capillary fringe thickness

Sample	Coordinates (x,y,z)	Median diameter (mm)	H_c (m)
2.6	72063.69,451827.95,0.71	0.400	0.181
3.5	72057.99,451803.99,0.76	0.402	0.180
4.3	72071.83,451826.11,0.92	0.406	0.178

These data suggest that the theoretical capillary fringe thickness is relatively constant in space, so in the data analysis H_c is assumed to be 0.18m. This is a fairly representative value: if at some location the grain size would be 0.3mm, H_c would be 0.24m, against 0.15m for a grain size of 0.5mm.

5. Results

5.1 Tidal oscillations in the groundwater level below the beach

Figure 5-1 shows the tidal signal as recorded by the Keller sensor in GW1, including the high and low water levels. The full time series of the other dipwells are shown in Appendix B. From the 11th of October onward (when all dipwells were installed), 24 tides were measured. From these tides and the accompanying high and low water levels, the amplitudes and asymmetry of the oscillations in the groundwater table are calculated. The results are discussed below.

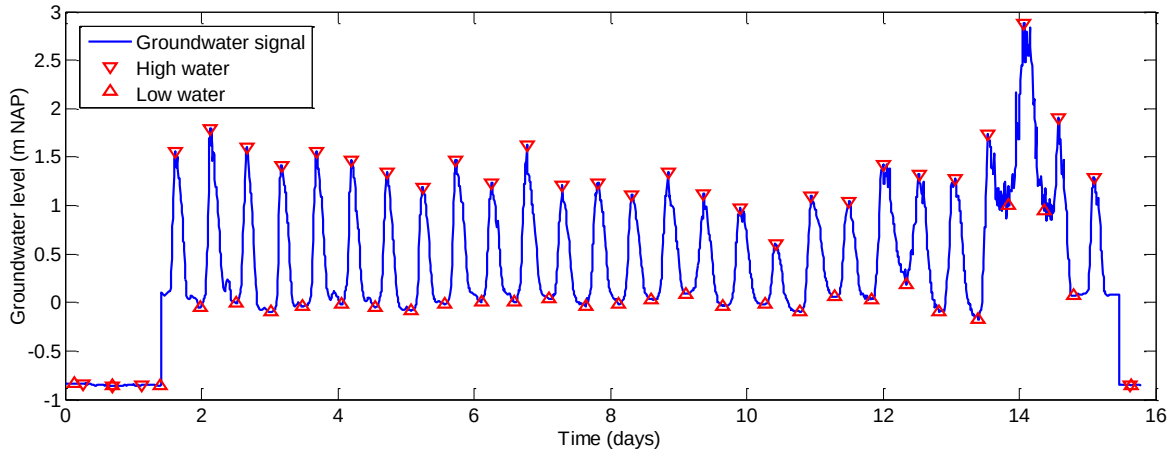

Figure 5-1. Groundwater table oscillations at GW1. Time is in days, with t=0 at October 9

5.1.1 Propagation of tidal oscillations into the beach

Damping

Figure 5-2 shows the decay of the groundwater amplitude over distance. The unconnected data point at x≈-20m gives the tidal amplitude based on the pressure transducer at this location (which on average is equal to 0.84m), whereas the connected points (x>-5m) are the water table amplitudes at the dipwells. According to Figure 5-2, the tidal amplitude in the groundwater is not decaying exponentially, as seen in literature. When only the first six dipwells are considered, the mean amplitude decrease appears to be exponential, but when GW7 and GW8 are included, the trend is more linear. This means that the location where no oscillations are visible anymore is on average only 10m landward of GW8 (at 78m from x=0). Only during neap tide (the lowest grey lines) an exponential decay in amplitude is visible.

In the dipwell 200m landward of GW1 (150m landward of the high water line), with the filter at 2-10m depth, groundwater oscillations are visible with an amplitude of approximately 5 cm, but they occur with a period of two weeks. This means that a frequency shift has taken place from a semi-diurnal tidal timescale to a spring-neap tidal timescale. A similar shift could not be observed in the time series of the dipwells, because the time of deployment of the sensors was too short to perform a variance density analysis.

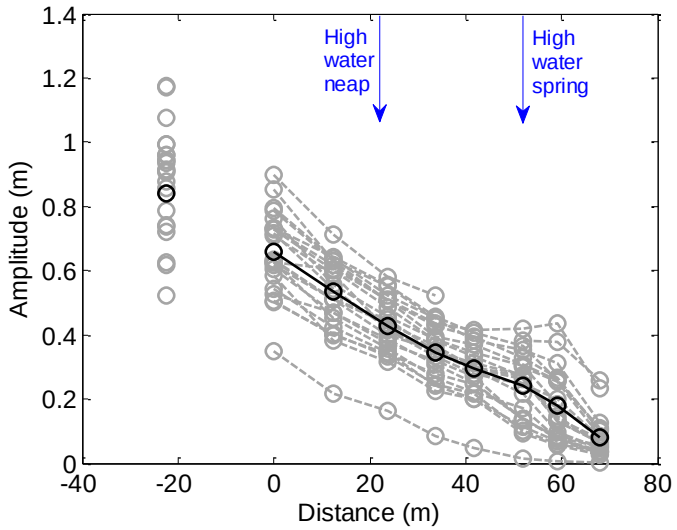

Figure 5-2. The decay of groundwater amplitudes over distance. The grey values indicate separate tides, whereas the black data indicate the mean.

Coupling and decoupling

It is interesting to note in Figure 5-2 that the amplitude at GW1 is on average of 0.25m smaller than the tidal amplitude. This observation is explained in Figure 5-3, which shows the tidal and groundwater signal during spring tide. It is visible that the tidal signal is somewhat sinusoidal, but in the groundwater, the falling tide is 'cut off'. At the moment when the tidal elevation and the groundwater level are not equal anymore, they are decoupled.

At GW1, the decoupling (at 8 and 20h) takes place when the groundwater level is still above the bed level. In the other dipwells, the decoupling takes place around the bed level. For example, GW3 is decoupled from the tide at 8h and 20h, at a level of +0.25m NAP, which is equal to the bed level at this location (right part of Figure 5-3). At GW3 and GW4, the decoupling takes place at +0.80m NAP, which is a little above the bed level of +0.55 and +0.70m NAP, respectively.

When the tide is rising, the tidal elevation and groundwater level are eventually coupled again, after which the groundwater level is 'forced' to go up with the tide. From this moment on, the sea surface elevation and groundwater level are equal. From GW3 landward, the coupling between tide and groundwater at rising tide happens at a lower SSE than the decoupling at falling tide. For example, the coupling in GW3 happens at 3 and 15h at an elevation of +0.3m NAP, while the bed level was +0.55m NAP. The distance between the coupling level and the bed level increases in landward direction. GW6, which has a bed level of +1.4m NAP, has a coupling level +0.8m NAP (at 3 and 15h). At GW1 and GW2, the coupling and decoupling levels are equal.

Since the coupling and decoupling are related to the bed level, they happen at an increasingly higher level relative to NAP when going inland. From this, the presence of the overheight can already be deduced, but the overheight will be further discussed in Chapter 5.1.2.

Another interesting feature in Figure 5-3 is found at 10h. The tide shows a minor peak here, which is visible with decreasing extant in the groundwater signals of GW1-GW3. Further landward, this peak is dampened out.

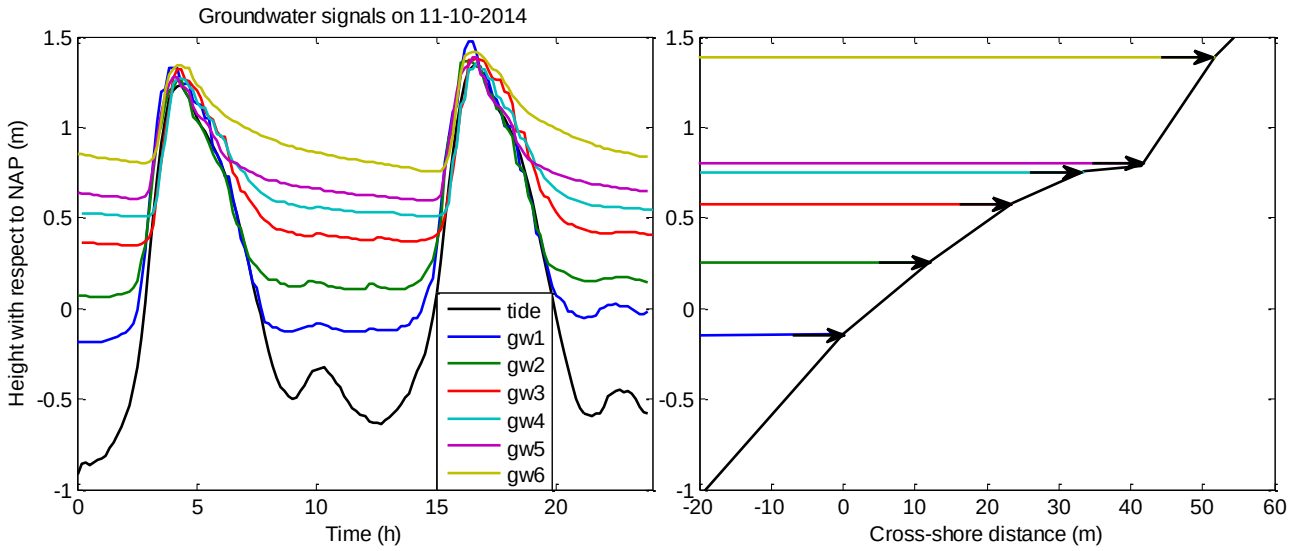

Figure 5-3. Comparison of the groundwater signals in the most seaward six dipwells with the tidal signal during spring tide

Figure 5-4, which illustrates the groundwater behaviour during neap tide, gives approximately the same result. Again, coupling and decoupling happen at the same level in GW1 and GW2 (+0.1 and +0.3m NAP, respectively). From GW3 to GW5, the coupling happens at a lower level than the decoupling, and the decoupling takes place at roughly the bed level. An example of this is GW4, where the coupling happens at 7 and 18h at +0.6m NAP, while the bed level and decoupling level are equal to +0.8m NAP.

The water level in GW6 is not being coupled to the tidal elevation in the first tide (between 5 and 10h). Yet, during the second tide, between 18 and 20h, the coupling takes place again. This might be due to the slightly larger tidal amplitude at this time.

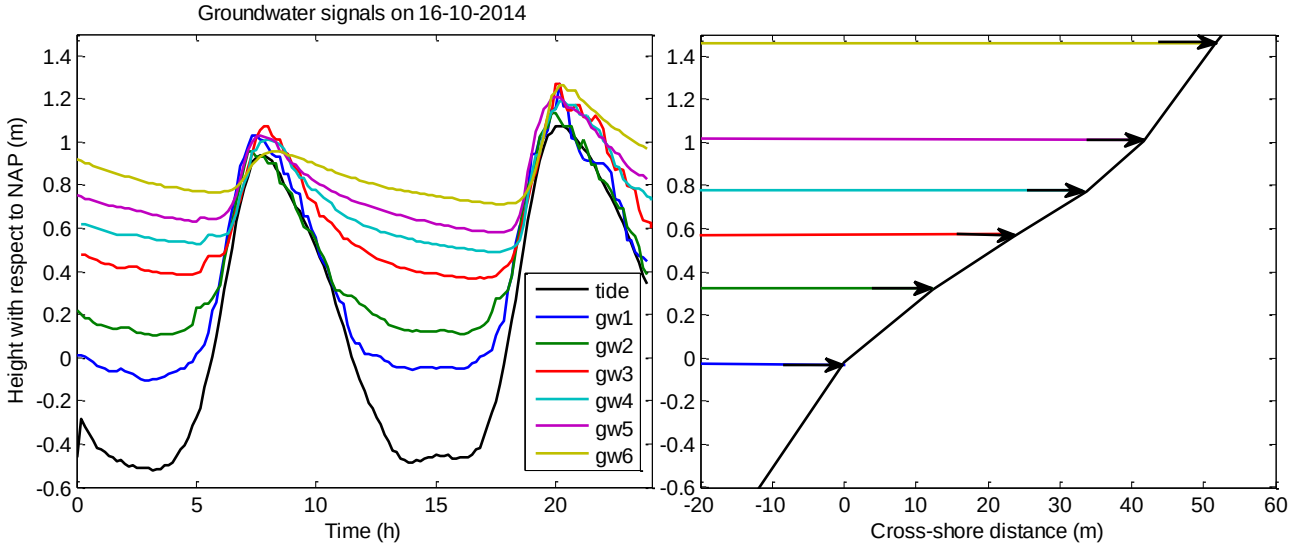

Figure 5-4. Comparison of the groundwater signals in the most seaward six dipwells with the tidal signal during neap tide

Time lag

During spring tide, GW6 is the first dipwell where the decoupling starts at high tide (Figure 5-3). During neap tide, the boundary is found more seaward, at GW5 (Figure 5-4). This is because these locations are approximately equal to the (high) water line during spring and neap tide, respectively (Figure 4-2). The groundwater fall at these locations is not related to the SSE fall anymore. Since

GW1-GW4 are always below the high water line, the occurrence of high water in the groundwater level in time is the same as the actual time of high water.

Higher up the beach, where the dipwells are never reached by the water line, the groundwater level and SSE are not coupled at all (Figure 5-5). This creates a time lag, which increases in landward direction. On top of that, the time lags are larger during neap tide than during spring tide.

The mean time lag between the tide and dipwells GW5 to GW8, measured over the entire deployment period of the sensors is given in Figure 5-6 (x-axis is the same as in Figure 5-1). Negative values are sometimes found due to difficulties in measuring the exact location of the high water level in time (for example at t=13). Yet, the figure clearly shows that the time lag increases with distance from the water line. On top of that, the time lag seems to increase during neap tide (around day 11, cf. Figure 5-1). The different dipwells do not give a uniform reaction to the storm that took place at t=14, even though the water level was far above the bed level of all dipwells.

The mean time lag at GW5 is 5 minutes, but this increases to 50 minutes during neap tide. This sensor is normally below the high water line, but during neap tide it is located just landward of the high water line. GW6, which is located 15m landward of the neap high water line and is equal to the spring high water line, has an average time lag of 20 minutes. Its neap tide peak is 90 minutes. For GW7, the mean time lag is 45 minutes, while it is located 5-20m from the high water line. The most landward dipwell, GW8, was located 15-30m from the high water line. The mean time lag at this location is 80 minutes, which increases to 190 minutes during neap tide.

In short, from GW6 landward, the time lag increases linearly with approximately 4min/m. The time lag increases when neap tide is approached, because the dipwells are further away from the high water line during neap tide.

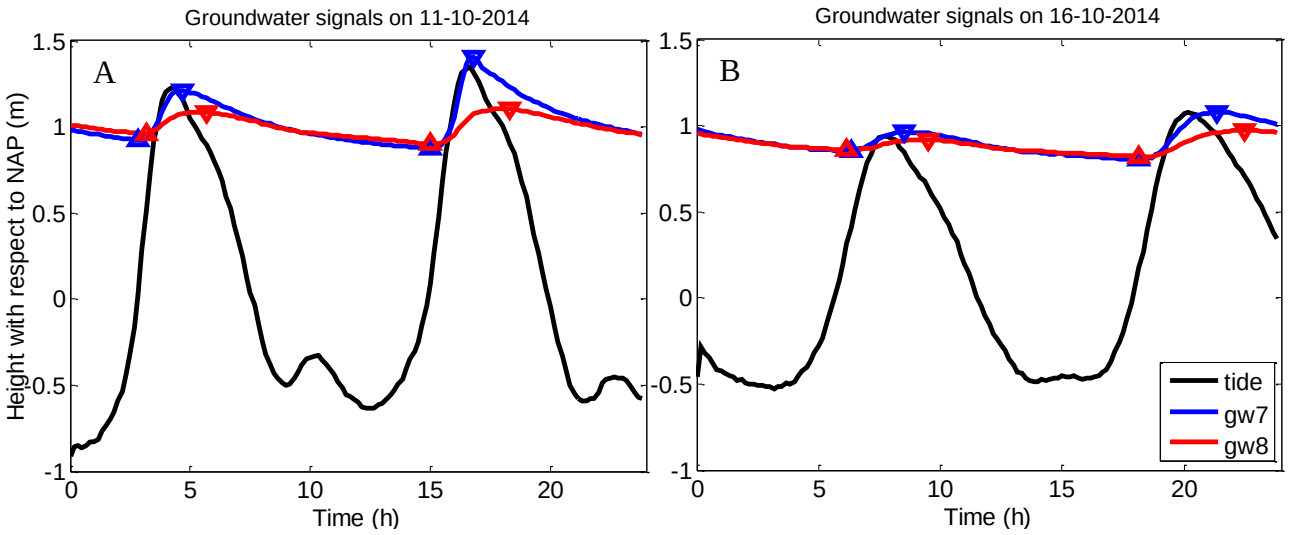

Figure 5-5. The groundwater signals of the two highest dipwells compared to the tidal signal, during spring (A) and neap (B) tide. Note the development of a time lag.

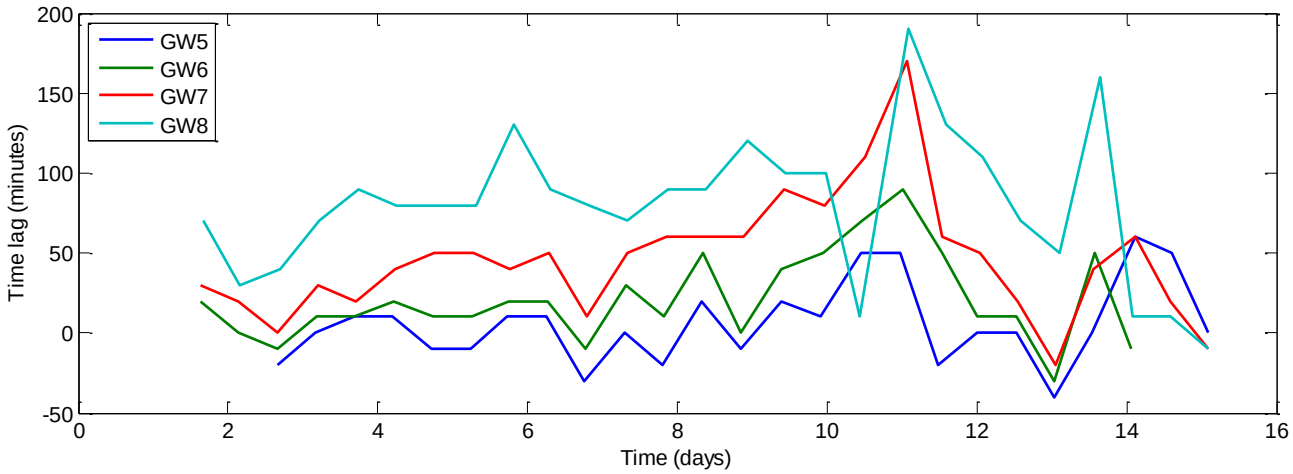

Figure 5-6. Evolution of the time lag throughout the deployment period of the dipwells. x-axis gives time in days, with t=0 at October 9.

Asymmetry

The change in asymmetry of the tidal (groundwater) waves over distance is given in Figure 5-7. As stated before, the tidal signal near the Sand Motor is quite asymmetric, with a short and fast rising tide and a much longer falling and low tide (Figure 4-3). This is confirmed by its average asymmetry value of 0.61 (at x=-22.5m). The first three dipwells (from x=0m to x=23m) show a gradual increase in asymmetry in the landward direction to 0.75. From GW4 landward, the increase in asymmetry slows down. The maximum average asymmetry is 0.82, which is found at GW6.

Landward from GW6, the asymmetry values decrease, to 0.73 in GW8. This trend has two causes. First of all, in the intertidal area (GW1-GW6) only the location of the low water level in time is delayed. In GW7 and GW8, the location of the high water level is also being delayed (the time lag), since at these locations, the tide and the groundwater are never coupled. Thus, time between low water and high water in GW7 and GW8 is thus longer, so the wave is less asymmetric (see Equation 8). Secondly, the amplitude of the groundwater signal is small in GW7 and GW8, which makes it relatively difficult to determine the location of the high and low water level (Figure 5-5).

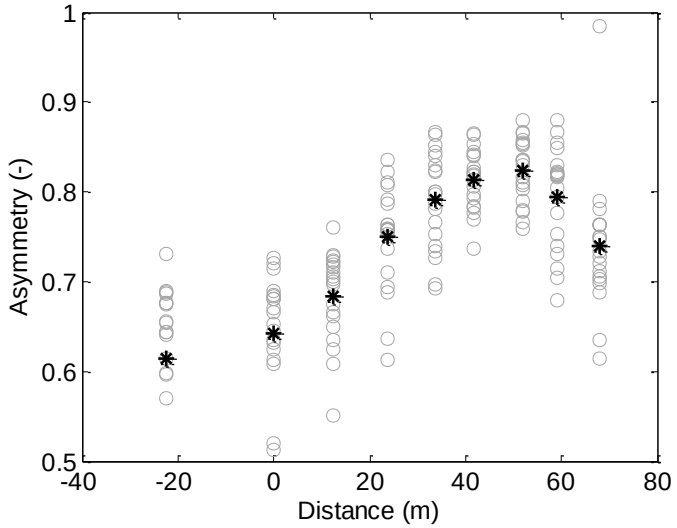

Figure 5-7. The evolution of asymmetry along the profile (grey are the values for each tide, black is the mean). Distance is relative to GW1.

5.1.2 The influence of the oscillating water table on the capillary fringe

Figures 5-3 to 5-5 have already shown that the inland water table is higher than the sea surface elevation, especially during low tide. This observation proves the existence of the overheight. A comparison of Figure 5-3 and 5-4 shows that specific differences exist between spring and neap tide. These differences are further assessed here.

Figure 5-8A shows that the overheight was clearly present on the 11th of October (spring tide). The figure shows the groundwater profile at low and high water. At low water, when the tidal elevation is approximately -0.6m NAP, the inland groundwater level is +0.9m NAP. At high tide, the inland water level is +1.0m NAP, which is lower than the SSE at that time (+1.2m NAP). The mean overheight is thus approximately +1m NAP.

Figure 5-8 also shows that the water table intersects the beach surface above the sea water level at low water. This implies the formation of a seepage face, but this was not observed in the field. There was no thin layer of water on present on the beach surface, but instead the surface was saturated.

Until approximately 40m inland, the water table is within 30cm from the beach surface, even at low water. Between 40 and 55m, the water table is only near the surface during part of the tidal cycle. From 55m landward, only above the high water line, the groundwater level is always more than 0.5m below the surface.

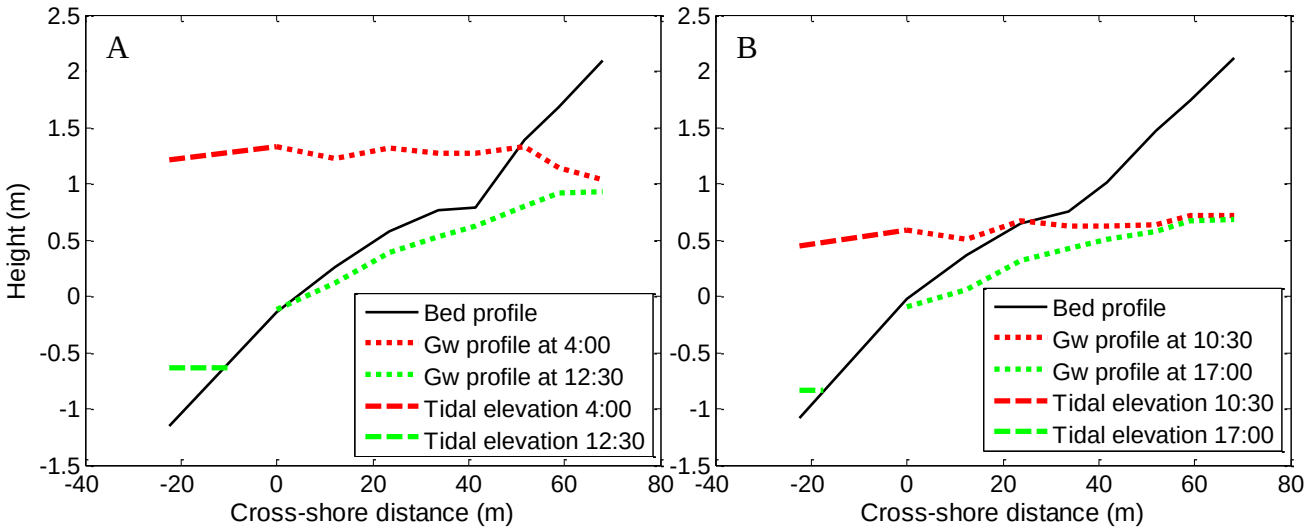

Figure 5-8. A: the overheight at different moments on the 11th of October (spring tide) B: the overheight at different moments on the 18th of October (neap tide)

Figure 5-8B shows the groundwater profiles during neap tide. Overall, the water table is further below the bed surface. For example, at x=20m, the distance between the water table and the bed surface during low tide was approximately 0.2m, whereas the distance at this same location increased to 0.4m during neap tide. Furthermore, the inland groundwater amplitude has reduced to nearly zero. The intersection of the beach surface and the water table is further away from the sea surface than at spring tide. The water table only intersects the beach surface at high tide approximately 20m inland, compared to 50m in the spring tide situation.

Another important observation from Figure 5-8 is the difference in overheight between spring and neap tide. The overheight is approximately 0.4m lower during neap tide than during spring tide. This value is larger than the daily groundwater amplitude at GW8, so it represents the spring-neap tidal variation in overheight.

From the above, it can be deduced that the capillary fringe can only be important for a limited amount of time during the day, and only on a restricted part of the beach. On top of that, the importance of the capillary fringe oscillates in a spring-neap tidal cycle. This is all visualized in Figure 5-9.

Figure 5-9A shows the amount of time during the day in which the water table is higher than -18cm below the surface. This represents the time that the capillary fringe could reach the surface, but also the time that the water level is above the bed level and will therefore prohibit aeolian sediment transport. The first observation is thatFigure 5-9 the amount of time that the water table is above -18cm is decreases in landward direction. This is due to the slope of the bed profile. A decrease is also found from spring to neap tide. This is explained by the fact that the high water level was nearly 1m higher during spring tide. This also causes the importance of the water table to reach further inland in this case. Another major difference between spring (October 11 and 12) and neap tide (October 18 and 19) is the presence of a peak at x=41.5m during spring tide. Toward neap tide, this peak diminishes. When this location is compared with Figure 5-8, it is visible that the bed surface flattens here. The overheight however, rises constantly in the landward direction. Therefore the water table is closer to the surface.

Figure 5-9B shows the amount of time per day that the capillary fringe can be of importance, since the water table is in between -18cm and the bed surface. There are two differences with Figure 5-9A. First of all, amount of time that the capillary fringe is of importance remains relatively constant in the first 35m. It only decreases more landward of this point. This is because the overheight runs more or less parallel to the bed level in these locations. Further inland, the overheight becomes horizontal, while the bed level still rises. This causes the capillary fringe time to decrease exponentially, and from 50m landward, the capillary fringe is no longer able to reach the surface. This is in accordance with Figure 5-8. Secondly, instead of one peak, there are now two peaks present during spring tide. The first peak (at x=12m) arises especially because the time that the water table is between -0.18m and the bed surface at x=0 is very small. This is because GW1 was located at the exit point during most of the low water, so the water table was higher than the surface. The other peak is the same as the peak in Figure 5-9A.

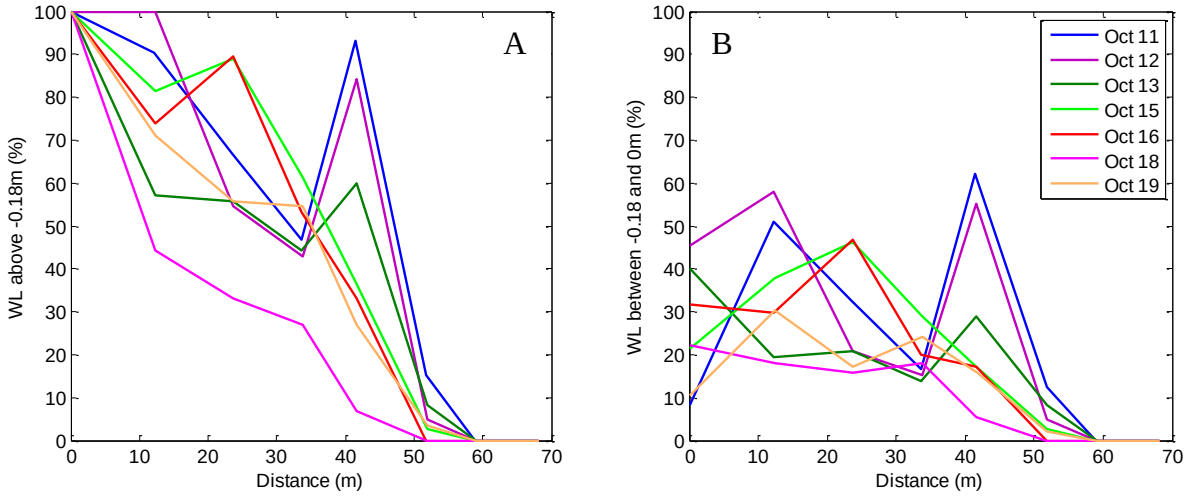

Figure 5-9. Importance of the capillary fringe. Left part (A) shows the amount of time per day that the water table is above -0.18m from the bed surface. Right part (B) shows the amount of time per day that the water table is between -0.18m from the bed surface and the bed surface.

The time lag mentioned in Chapter 5.1.1 was also considered in the case of the overheight. Figure 5-5 showed that the groundwater level at GW8 rises and falls later than the groundwater level in GW1. This means that the importance of the capillary fringe will also rise later in time. This is visualized in Figure 5-10, where the groundwater profiles of the beginning of low water and halfway through flood are plotted of the 12th of October. It is visible that at the seaward part of the bed profile the groundwater level is rising, while at the same time at landward part of the bed profile the groundwater level is falling.

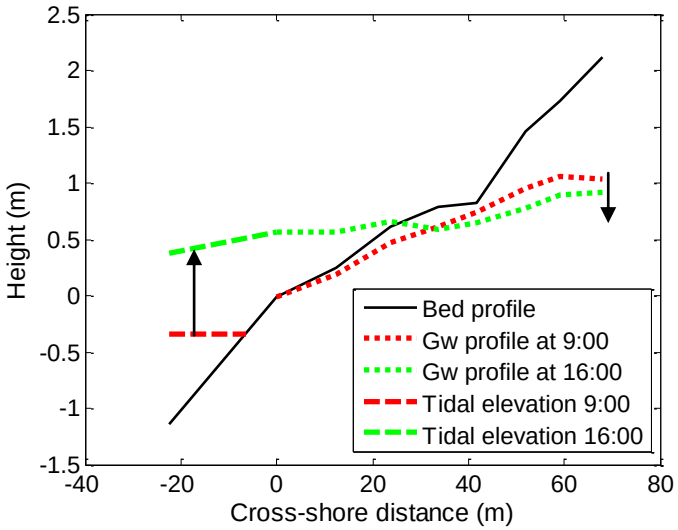

Figure 5-10. Visualization of the time lag in the overheight for the 12th of October

5.2 Effects of oscillations in the groundwater table on the surface moisture content of the beach

Now the effect of the tide on the groundwater level in the beach is discussed, the focus of the study is shifted toward surface moisture content. This chapter will discuss the interaction between the water table and the surface moisture content. Other possible influences, like precipitation, evaporation and bed surface slope are also assessed.

5.2.1 Surface moisture variations on tidal timescales

Spring tide

The variations in surface moisture content are compared to the water table elevation during two parts of the tidal cycle: spring tide and neap tide. First, spring tide will be discussed. Figure 5-11 shows the behaviour of the moisture content, the water table depth and the tidal elevation on the 12th and 13th of October. The combination of these two days gives an impression of an entire tide (from one high water to the next). The water table depth is given as the distance between the bed surface and the water table, and is therefore positive if the water table is below the bed level. If the depth is negative, the water table is above the bed.

On October 12, the surface moisture measurements can clearly be divided into three groups. GW1, GW2 and GW5 are constantly wet, with moisture contents of 18% and higher. These locations were submerged during high tide, and the water table is always within 18cm from the surface. Halfway through low tide, the surface moisture content decreases, but especially at GW1 and GW2 it increases again when the tidal elevation increases. At GW5 this does not happen, which is probably due to the fact that this location is further away from the water line and the water table reacts later to the rising sea surface.

At GW3 and GW4, the surface moisture content decreases from high water to low water. The surface moisture content at GW3 is higher than at GW4, corresponding with the deeper water table at GW4. The water table is between 5 and 30cm depth in these locations. This corresponds to a decrease in moisture from 25% to approximately 8% moisture.

GW6, GW7 and GW8 are characterized by their low surface moisture contents. The water table near GW7 and GW8 is constantly more than 40cm below the surface. The water table at GW6 is only 5cm from the surface at high water, but when the measurements started, it was 40cm below the surface. The highest surface moisture contents are found near GW8, but the differences between the three dipwells are within the standard error of the theta probe, so they are not significant.

On October 13, when rising tide was studied, the results are not strongly grouped anymore. Yet, the trends follow those of the previous day. GW1, where the water table is always within 6cm from the surface, is always saturated. GW2 and GW5 are very similar concerning both surface moisture and depth of the water table. As the water table slowly falls, the surface moisture content decreases to approximately 13% moisture at a water table depth of 25cm. When the tide starts rising, the decrease in water table depth is accompanied by an increase in surface moisture content. Again, since GW5 is further away from the water line, the water table and surface moisture content at this location start rising a little later than at GW2.

During the measurement period, the water table depth at GW3 and GW4 is nearly identical, 29cm for GW4 and 25cm for GW3. Surface moisture contents are on average 3% moisture apart, but do not show a clear trend.

GW6, GW7 and GW8 are still below the critical value for aeolian transport of 10% moisture. Again, the highest surface moisture content is found at GW8. In this case it is approximately 3%

moisture higher than the moisture content at GW6, which is higher than the standard error of the probe. Still, throughout the measurement period, all these dipwells are more than 50cm below the surface. Thus, the differences between these three dipwells cannot be assigned to the depth of the water table.

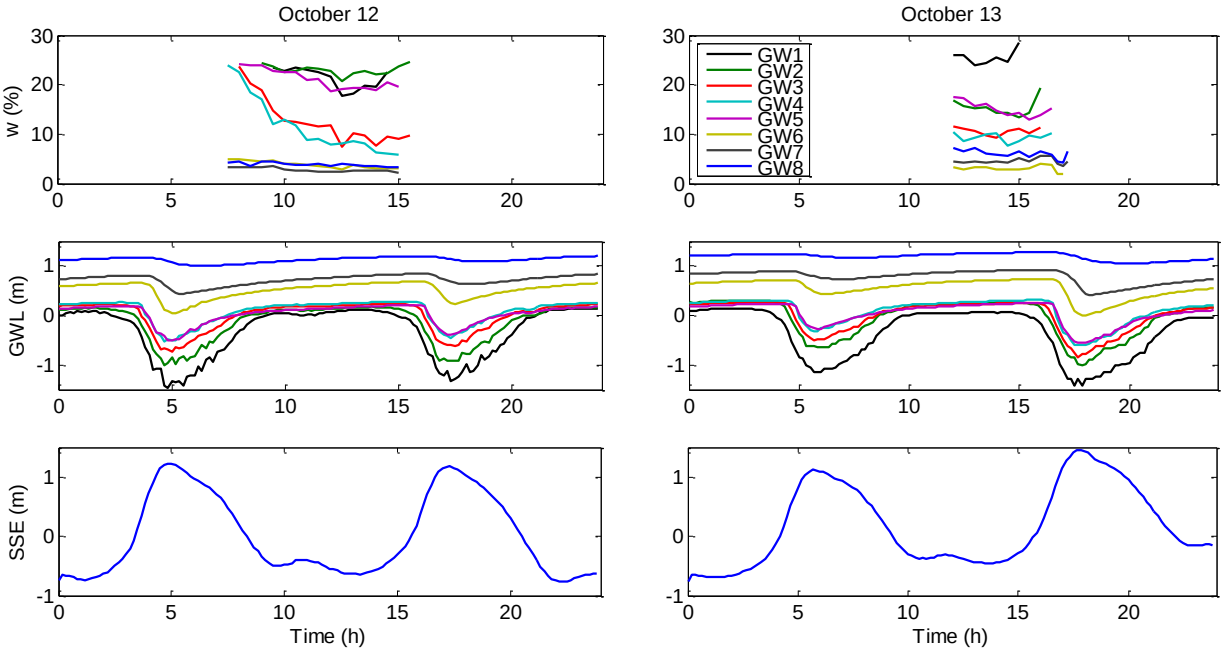

Figure 5-11. The interaction between tidal elevation, depth of the groundwater level and surface moisture content during spring tide. GWL is depth of the water table, in m below the surface (so negative values indicate that the water table is above the surface).

Neap tide

Tides, groundwater depths and surface moisture contents on October 16 and 18 are plotted to study an entire tide from high water to high water during neap tide (Figure 5-12). Starting from high water (at October 16), it is visible that GW2 to GW5 now show a trend comparable to GW3 and GW4 in Figure 5-11. As soon as the water table falls below the bed surface, the moisture content at that particular location decreases. With increasing distance from the water line, the surface moisture content decreases more. This is related to the depth of the water table. The decrease at GW3 for example stagnates at 17% moisture, when the water table is 17cm below the surface. GW5 decreases to 9% moisture, with a water table at 35cm depth. The water table was at the same depth at GW2 and GW3 between 12 and 14h, but at GW2 the it fell below the surface later in time, so the drying process started later and no equilibrium could be reached.

During rising tide, only GW2, GW3 and GW4 show a clear trend. When the water table rises to 23cm from the bed surface, the surface moisture content starts to increase. At GW2 and GW3 the water table rises to above the bed surface, which thus becomes saturated. At GW4 however, the maximum elevation of the water table is within 13cm of the surface. The surface moisture content rises accordingly. When the water table falls deeper again, the surface moisture also decreases.

In spite of a water table at 40cm depth, the surface moisture content at GW5 is relatively constant at 6-9% moisture. This is relatively moist, and cannot be explained by the water table elevation. This also applies to GW6 for rising tide.

At GW1, the water table never got lower than 3cm below the surface, and the surface was therefore always saturated. GW7 and GW8 were always dry, corresponding to the fact that the water table was always more than 50cm below the surface.

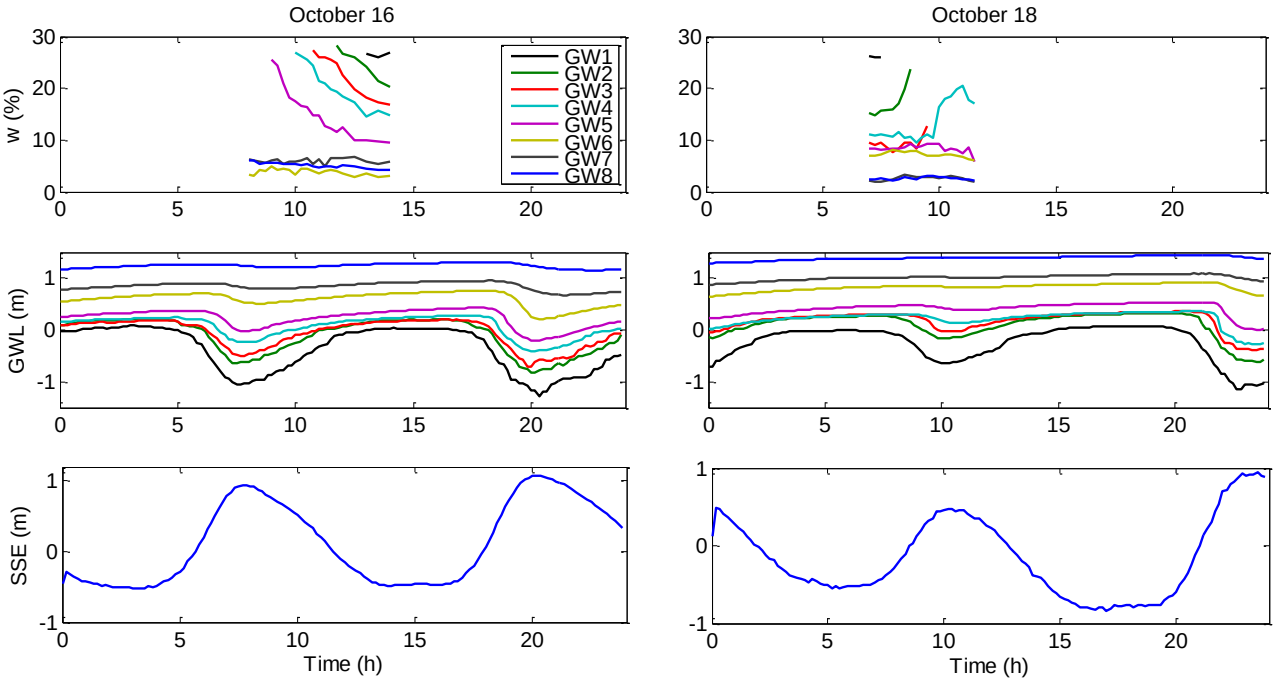

Figure 5-12. The interaction between tidal elevation, depth of the water table, and surface moisture content during neap tide.

Overall trends

When the evolution of surface moisture content over a tidal cycle during spring and neap tide is compared, several observations are made. First of all, the falling tide is better recognized in the surface moisture content. During both spring and neap tide the locations that are at or below the high water line show a clear drying curve. When the water table falls deeper below the surface, the final surface moisture content is lower.

When the tide rises again, the increase in surface moisture content is smaller. Only a little increase is achieved before the surface is inundated. This increase commonly starts at approximately 15m from the water line. The decrease in surface moisture content during falling tide is found in GW1-GW5, while the increase is only found in GW1-4.

From Figures 5-11 and 5-12, it is still hard to determine the actual depth of the capillary fringe. Therefore, all surface moisture contents are now plotted together with the depth of the water table at the time they were measured (Figure 5-13). The measurements were done from spring to neap tide (October 11 to 19), alternately during rising and falling tide.

Figure 5-13 shows a very clear pattern. The surface is saturated when the water table is within 10-20cm from the surface, and dry when the water table is 35cm or more below the surface. When the water table is between 10 and 30cm below the surface, a range of moisture contents between 10 and 23% moisture is found. The depth at which the surface is saturated is equal to the thickness of the capillary fringe. On average, the capillary fringe thickness is thus 15cm, which is very similar to the calculated thickness of 18cm.

The thickness of the capillary fringe is smallest during spring tide. This might be related to the faster rise of the water table during spring tide. When the water table rises quickly, the top of the

capillary fringe will initially remain at the same level. In this case (especially in GW3-6) the rise of the water table is so fast that it is not possible for the capillary fringe to rise along, to create a new stable equilibrium.

There is no clear evidence that the rise and fall of the water table are matched with differences in rising and falling surface moisture content (hysteresis). The wetting curves (for rising tide) seem to be a little lower than the drying curves (falling tide). However, this might also be due to the approaching of neap tide.

It can be concluded that the water table can have a significant influence on the surface moisture content as long as it is within 30cm from the surface. Figure 5-13 shows that the zone below this, between 30 and 50cm, is still characterised by a small range of 5 to 12% moisture. Within this range the critical threshold for aeolian sediment transport is located, so the cause of the variation in surface moisture still has to be found. The first explanation might be slow drainage to the water table, but the higher surface moisture contents are also found during rising tide. Another explanation might be precipitation, which can increase surface moisture content irrespective of water table elevation. The effect of precipitation and evaporation will thus be considered in the next paragraph.

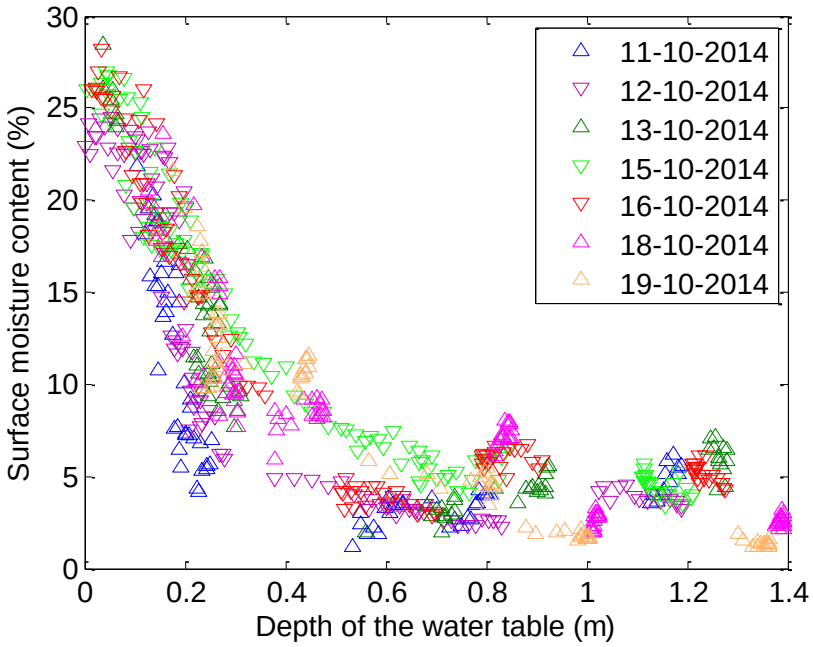

Figure 5-13. Dependence of surface moisture content on the depth of the water table. Depth is given in m below the surface. Δ represents measurements done during rising tide, ∇ represents measurements done during falling tide.

5.2.2 The effects of precipitation and evaporation on surface moisture content

Even though some variations in surface moisture content can be ascribed to variations in the groundwater level, other potential causes are not yet excluded. It is possible that the surface moisture content is influenced by the prevailing meteorological conditions. Therefore, the behaviour of the surface moisture content is now compared to precipitation and evaporation.

On October 11, surface moisture measurements were done throughout the last part of low water (Figure 5-14). A little precipitation had fallen just before the measurement period, and more rain fell in the middle of the measurement period. Due to a complete overcast, evaporation was small, and only increased after the larger precipitation event (at 13:00). The surface moisture content at GW1, 3, 6, 7 and 8 increased after the larger precipitation event. At GW5, only a very small increase is

found, but this is followed by a decrease. No significant decrease in surface moisture content is visible with respect to the evaporation after the rain had ceased.

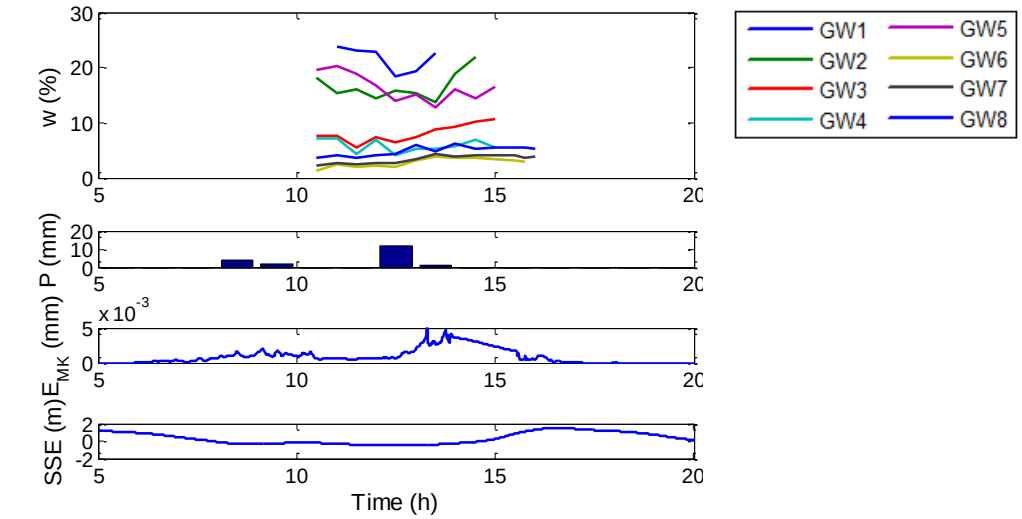

Figure 5-14. Surface moisture content (w), meteorological conditions (precipitation P and evaporation EMK) and tidal elevation (SSE) on the 11th of October

On October 13, precipitation fell just after the beginning of the measurements, while the tidal elevation was still low (Figure 5-15). The amount of rain was smaller than on October 11. Evaporation was very small during the entire measurement period, so a decreasing moisture content (e.g. at GW5) cannot be ascribed to it. GW1 and GW4 show increasing surface moisture contents at the same time of the precipitation event, but the surface moisture content was already rising at GW4 before precipitation fell. GW3 and GW8 experience a slight decrease, and the surface moisture contents at GW2, 5, 6 and 7 remain the same.

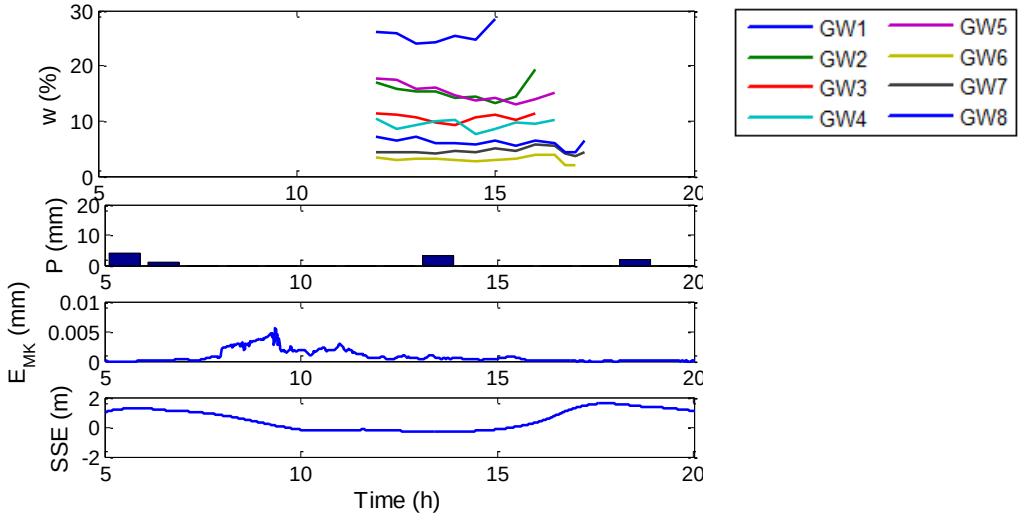

Figure 5-15. Surface moisture content (w), meteorological conditions (precipitation P and evaporation E_{MK}) and tidal elevation (SSE) on the 13th of October

On October 16, the highest amount of precipitation was measured. Especially the surface moisture contents at GW6, GW7 and GW8 are interesting, since the rain had fallen before the measurement period (Figure 5-16). The other dipwells were still submerged at that time, so the drying that is visible can also be ascribed to drainage to the water table. Curiously, GW6 is even

lower in moisture content than GW7 and GW8. GW8 is the only location where an apparent drying process is taking place, but the decrease is very small and within the standard error of the theta probe. This means that it is not significant.

The moisture content at GW6 is lower than the moisture content at the same location on October 18 (Figure 5-12), even though it was neap tide on October 18 and the water table was further away from the surface. At GW7 and GW8, moisture content is higher than on October 18. This could not be explained by the depth of the water table, since it was approximately 1m below the surface. The moisture content at GW7 and GW8 might thus be explained by the precipitation event.

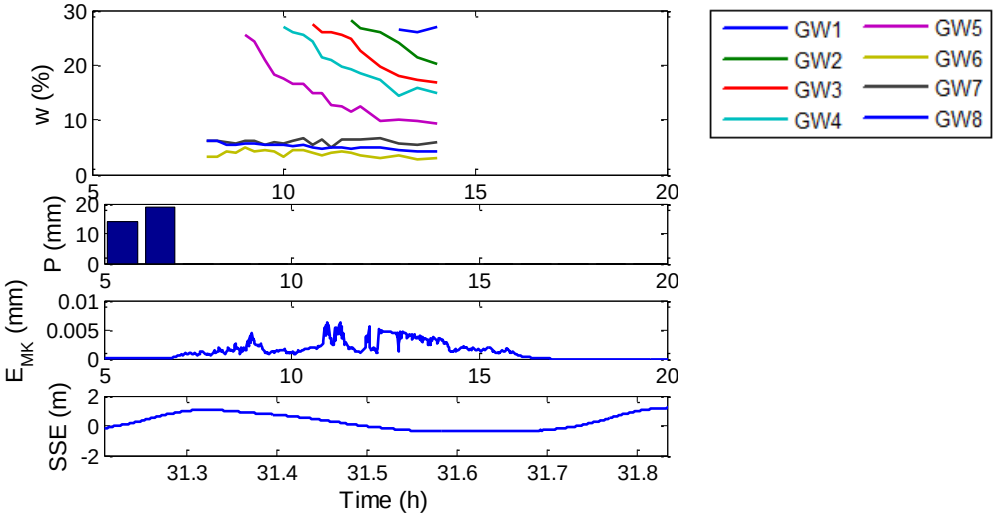

Figure 5-16. Surface moisture content (w), meteorological conditions (precipitation P and evaporation E_{MK}) and tidal elevation (SSE) on the 16th of October

5.2.3 The effect of the beach slope on surface moisture content

It was hypothesized that the surface moisture content would be influenced by the beach slope. With a higher slope, the groundwater level at a certain distance inland is lower than with a lower slope (Raubenheimer et al., 1999; Ataie-Ashtiani et al., 2001). Figure 5-9 in Chapter 5.1.2 has already demonstrated that the capillary fringe will be less likely to reach the surface, so the surface moisture content will be lower.

To test the hypothesis, two days with different bed profiles are compared (Figure 5-17 and Figure 5-18). They are one spring-neap cycle apart, so the tidal elevation at low tide and the submersion history per dipwell is approximately the same. Up to a distance of 13m, the beach slope on September 28 is higher than that of October 13. At the same distance, it is visible that the surface moisture decreases much faster on September 28. From 13m landward, the beach gradient reverses on September 28, and the surface moisture content immediately increases. On October 13 however, the gradient becomes slightly smaller, and the decrease in surface moisture content stagnates. This pattern is also found on September 28, from 50m landward. The high gradient corresponds with a rapid decrease in moisture content, and when the gradient decreases, the decrease in surface moisture content slows down. On October 13, the surface moisture increases when the bed level becomes horizontal (at 40m), but remarkably also at 70m, where the gradient of the bed surface is not changing.

These observations imply that a higher beach slope indeed results in a lower surface moisture content, which confirms the hypothesis. The explanation is found in the 'constant' slope of the

groundwater table. This slope is independent of the slope of the beach surface, so when the beach surface slope decreases, it immediately approaches the water table.

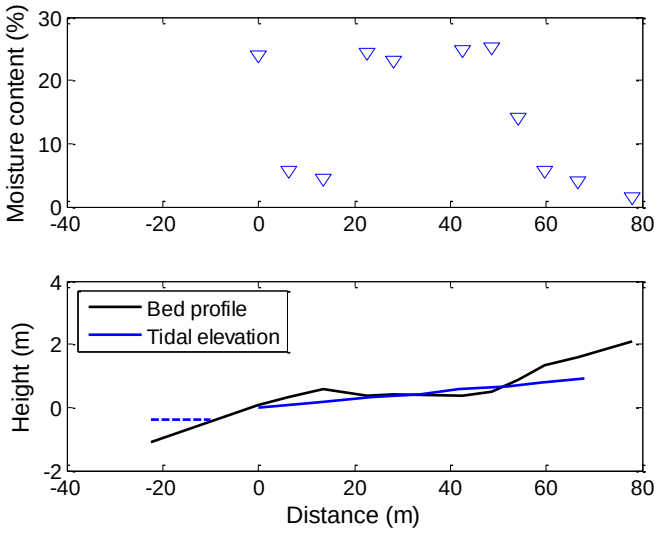

Figure 5-17. The bed profile on September 28, and the corresponding surface moisture content at low tide

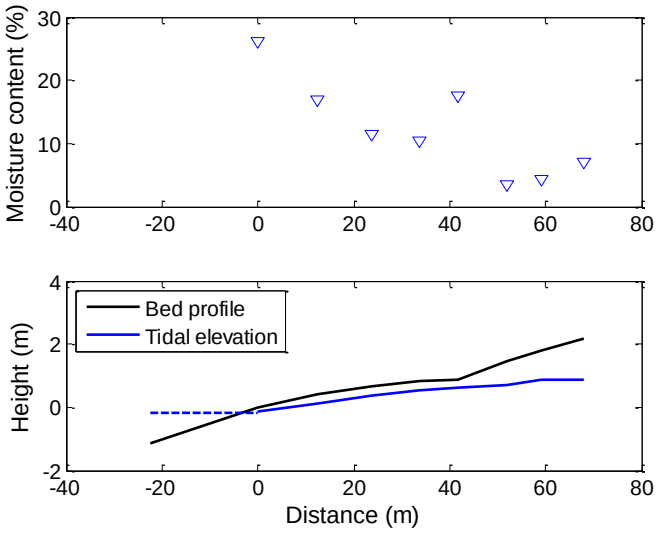

Figure 5-18. The bed profile on October 13, and the corresponding surface moisture content at low tide

5.2.4 The relative importance of the tide in determining surface moisture content

By combining Chapter 5.2.1 to 5.2.3, the relative importance of the tide in determining the surface moisture content can be defined. In chapter 5.2.1 it was found that the capillary fringe thickness at the Sand Motor is approximately 15cm. However, the tide will be able to affect the surface moisture content as long as the water level is within 30cm from the bed surface.

The influence of precipitation and evaporation on surface moisture content is still unclear. In the studied cases, the changes in surface moisture content after precipitation and evaporation events were at least smaller than the changes due to the tidal oscillations in the water table.

Since the slope of the water table is relatively constant, the distance between the water table and the bed surface is strongly dependent on the slope of the bed surface. This causes a low surface moisture content at high beach slopes, and higher surface moisture contents at lower slopes.

6. Discussion

6.1 Comparison of results with literature

At the Sand Motor, the decay of the groundwater amplitude is not always exponential, as hypothesized and suggested by literature (e.g. Liu et al., 2012). In the present study, it was found only to be exponential during neap tide. Especially above the high water line an unexpected rapid decrease in amplitude is found. Only two explanations exist for this observation: either the beach gradient suddenly decreases (which leads to more dampening, as described by Mao et al. (2006)), or the sediment grain size has become smaller. A smaller grain size will reduce the hydraulic conductivity of the sand, and the (tidal) wave will therefore experience more dampening (Baird and Horn, 1996). Figure 4-2 shows that the beach gradient at GW7 and GW8 does not differ significantly from the gradient at GW6, so the gradient cannot cause the sudden amplitude decrease. In a situation with a natural beach, an abrupt change in grain size is not to be expected either, but in the case of the Sand Motor, the beach was not formed by natural processes. Therefore, it is possible that a layer of fine sand is present near GW7 and GW8, which reduces the groundwater amplitude.

The coupling and decoupling that were found between the tide and the water table (Figure 5-3 andFigure 5-4) are explained by existing literature (e.g. Turner, 1993): the hydraulic conductivity of the sand acts as resistance for the tidal wave. As soon as the falling water table equals the bed surface, the groundwater level cannot fall as fast as the sea surface anymore, so decoupling takes place. The coupling takes place at a certain distance below the bed surface, because it is easier for the water to infiltrate at rising tide, since the flow is mostly vertical. Exfiltration happens as a consequence of the hydraulic gradient, which is smaller during neap tide. Thus, the groundwater falls slower than the tide, so decoupling happens earlier. Infiltration is also slower during neap tide, because the high tide level is lower than during spring tide. Since infiltration is governed by gravity (or the height of the water column above the bed), the total infiltration force is smaller during neap tide. The decoupling at or above the bed level might indicate the formation of a seepage face, where the exit point of the water table is higher than the SSE. Yet, this was not found in the present study.

The time lag between the tide and GW8 was found to be 80 minutes, and the tidal period is 12 hours and 20 minutes (or 740 minutes). This means that the phase difference between the tide and GW8 is 80/740=0.11. This is smaller than the 4 hours (phase difference of 0.32) which were found by Pollock and Hummon (1971). Another difference is that Pollock and Hummon (1971) found this time lag around the high water line, while the present study found a maximum time lag of 50min (phase lag 0.07) at the high water line. An explanation for this is found in the beach slope: the present study was executed on a beach with a slope that was approximately four times smaller than the beach in the study of Pollock and Hummon (1971). On top of that, the grain size in the present study area was four times larger. The linear increase of the time lag with distance was found, but only in the three most landward located dipwells, since they are above the high water line for a large part of the spring-neap tidal cycle.

The landward increase in asymmetry of the groundwater oscillations at the Sand Motor is comparable to the increase that was found in the study of De Groot (2002). In both cases, the asymmetry increase was approximately linear in the first 40m of the intertidal area (0.7 to 0.9 at Egmond, and 0.65 to 0.82 at the Sand Motor). More landward, the present study found a decrease in asymmetry, which was not found before, since previous research on this topic was restricted to the intertidal area.

At a borehole 200m landward of the measurement array (for the study of S. Huizer, Utrecht University), a clay layer was found at approximately -7m NAP. When this layer is assumed to be the aquifer boundary, and the tidal amplitude is assumed to be 0.84m, Equation 1 returns an average overheight of +0.016m NAP. This is highly unrealistic, since commonly (on other beaches) values of 1-2m were observed. The present study confirms this, as the overheight was found to be approximately +1m NAP. This implies that the beach slope is very important, as already suggested by Turner et al. (1997).

The intersection between the water table (excluding the capillary fringe) and the beach, that was found to be higher than the tidal level at low tide during both neap and spring tide (Figure 5-8), could be explained by the formation of a seepage face, but this was not observed in the field. Instead, the high groundwater level might be explained by the presence of short waves (sea, swell and infragravity waves). They can create a set-up of 40% of their offshore wave height, which is superimposed on the tidal level (Turner et al., 1997). At October 11, wave height was approximately 0.6m, so the maximum set-up would be 0.24m. Yet, the intersection of the water table with the beach was 0.5m higher than the tidal level (Figure 5-8). At October 18, wave height was 1.3m, so maximum set-up would be 0.52m. The intersection of the water table with the beach, however, was 0.8m above the tidal level (Figure 5-8). This means that the presence of the high intersection can only partially be explained.

When only the water table and associated capillary fringe elevation were considered, not all variations in surface moisture content could be explained. This is especially the case at locations higher up the beach, where the water table is more than 30cm below the surface. The variations that are found here might be explained by meteorological conditions, like precipitation and evaporation, as hypothesized. Nevertheless, the hypothesis could not be confirmed. The night before October 13, a lot of rain had fallen, but the surface moisture content at the locations where the water table did not reach the surface do not show any higher outcomes than in a dry situation (Figure 5-15). The same result was found on October 16 (Figure 5-16). No significant prove was found for the effect of evaporation either, which is in accordance with the findings of Schmutz (2014), who already stated that evaporation is most important at the saturated part of the beach. However, at these locations drainage (to the water table) is much more important than the few millimetres of water that evaporate during a day. Yet, another meteorological process was found during the field campaign to affect the surface moisture content. On October 13 a strong wind was blowing, and thus causing aeolian transport. The (dry) sediment was deposited near GW6 and GW7, and accordingly, the surface moisture contents at these locations on this day are very low (Figure 5-15).The above implies that the groundwater level (induced by tidal oscillations) is more important in determining the surface moisture content of the upper 2cm of the bed than both precipitation and evaporation.

Together with the groundwater level, the beach surface slope is found to be very important in determining surface moisture content for the conditions experienced here (Figure 5-17 and Figure 5-18). The hypothesis that a higher slope would result in lower moisture contents (which was based on previous research by Raubenheimer et al. (1999) and Ataie-Ashtiani et al. (2001)), was validated. Only a small increase in slope resulted in a surface moisture content decrease of more than 10% moisture. During a tidal cycle, the surface moisture variations can be in the order of 20% moisture. Therefore, it can be stated that the tide is the most important factor in determining the surface moisture content on a beach, but the slope is almost of equal importance. This is due to the more or less linear slope of the groundwater table, which is unaffected by the bed slope on the spatial scale considered here.

6.2 Implications of the results for aeolian sediment transport

When Figure 5-9 is studied, it is evident that the capillary fringe is most important during spring tide. The combination of the high water levels (inundating the beach) and the closeness of the capillary fringe to the surface should prohibit aeolian transport for most of the day across almost the entire profile. This is confirmed by the actual surface moisture contents.

Since the overheight was +1m NAP, and the maximum capillary fringe influence was 30cm, the capillary fringe is thus important when the bed level is below +1.3m NAP. For the Sand Motor, this is equal to the intertidal area. If the slope of the beach above the high water line would have been lower, the effect of the capillary fringe on the surface moisture content (and therefore on aeolian sediment transport) would have reached further inland.

When the variations of the surface moisture content are compared to the oscillations in the groundwater level, several observations are made. First of all, the surface moisture content at GW1 is nearly always higher than 20%, and the lowest value that is reached in GW2 is approximately 15% moisture. This means that the sediment is not available for aeolian transport at these locations at any time during the tidal cycle. From GW3 landward, values below 6% moisture are sometimes reached. Thus, only at these locations aeolian sediment transport is (sometimes) possible. It is found that the boundary where the surface is dry enough for aeolian transport is oscillating on a spring-neap tidal time scale. The surface moisture content at GW6, 7 and 8 (10 to 30m landward of the high water line) is always below the threshold for aeolian sediment transport. This is caused by the depth of the water table, which is always more than 30cm.

In the case of the rising tide, the surface moisture increases in some cases, but only when the moisture content was already above the threshold for aeolian transport. In all other cases, it was found that the surface keeps drying until it is suddenly inundated by the rising tide or sea- swell- or infragravity waves.

6.3 Reliability of the data and suggestions for further research

200m landward of the dipwell array, at a depth of 16-20m below the beach surface, oscillations with tidal frequency and an amplitude of approximately 0.15m are found. However, this does not necessarily refute the results from the present study, since this is probably due to the presence of horizontal clay layers. They can form a second aquifer at this depth, with different characteristics than the upper aquifer. These characteristics include grain size and hydraulic conductivity, which make it possible that waves can travel further through the beach. However, at this depth the oscillations are not relevant for aeolian transport. It was also found that in this dipwell, the overheight is on average +1.45m NAP. This is in accordance with the present results: it is highly plausible that the overheight rises with 0.5m in the 200m landward from the measurement array.

Most of the surface moisture variations in dipwells GW6 to GW8 are within 1.5% moisture, so they can be ascribed to the standard error in the measurements. Some of the larger variations in moisture content cannot be ascribed to this, while it is also unlikely that the surface moisture was really varying at this small time scale. An explanation might be found in the beach surface characteristics. Sometimes, sea shells make it hard to do the correct measurements with the probes. It was noted in the field that shells cause the probe output to be lower than expected (so the moisture content is underestimated). Organic matter has the opposite effect: a small layer of organic matter (e.g. algae) on the beach surface might give a significantly higher probe output than expected. This is a possible explanation for the high ‘moisture content’ at GW8 in Figure 5-11.

The fact that the present study could not find any effect of precipitation on surface moisture content does not mean that this effect is nonexistent. Rain fell only on a very few days during the field campaign, so the effect could not be studied thoroughly. On top of that, the precipitation measurements should be in mm/min instead of mm/hour in order to find a relation, since the surface moisture measurements were done more than once per hour.

The use of a terrestrial laser scanner could improve the surface moisture measurements, by measuring a large area and only the top few millimetres of the sediment (Nield et al., 2011). This is especially important when the effect of precipitation on surface moisture is included. The Delta T theta probe that was used in the present study averages the output over 2cm, which may not be representative of the actual surface moisture content. It was found that the probe would still give a dry output, even if the top layer of sand was wet due to the rain. According to the probe, aeolian sediment transport would thus be possible, but in reality this was not always the case. Therefore, the use of a terrestrial laser scanner is suggested for further research.

7. Conclusions

1A. What changes are experienced by the tidal wave when it propagates through the beach?

At the Sand Motor, the semi-diurnal tidal oscillations are found up to 80m from the water line, which is equal to 30m landward from the spring high water line. Along the same distance, the tidal signal becomes more asymmetric. A time lag between the tidal signal and the water table arises landward from high water line. With an average increase of 4min/m, the time lag at 20m from the high water line is 80min.

1B. How far into the beach is the water table high enough for the capillary fringe to bring water to the surface?

The overheight at the Sand Motor is approximately +1m NAP, and the maximum influence of the capillary fringe is found at a water table depth of 0.3m. The overheight is higher during spring tide than during neap tide. Therefore, the capillary fringe is estimated to reach the beach surface for a longer time throughout the day during spring tide. At the Sand Motor, the capillary fringe can only affect the surface moisture content in the intertidal area.

2A. Until what height above the high water line is surface moisture variable with tidal frequency?

If the water table remains within the 30cm from the bed throughout a tidal cycle, the surface moisture content can be stopped above 10% moisture. If the water table falls to below 30cm from the bed, or does never even reach this high, the surface moisture content can decrease to below 10% moisture: a level that is low enough to initiate aeolian transport.

Above the high water line, no distinct variations in surface moisture content were found. Yet, during spring tide the surface moisture content is affected higher up the beach, since the overheight is higher. The spring-neap tidal cycle has a large influence on the surface moisture content and thus presumably on aeolian sediment transport.

2B. What is the relative importance of the tide in determining surface moisture content?

The tide was found to be the most important factor in determining the surface moisture content. In the present study, precipitation and evaporation were found to be of very small importance. Instead, the beach slope is another strong factor in determining surface moisture content. This is due to the slope of the water table, which is independent of the beach surface slope, and only depends on tidal amplitude. If the beach slope is low, it might therefore intersect the water table, and if the beach slope is high it will have a larger distance to the water table.

Main question: What is the relation between tidal oscillations in the water table and variations in surface moisture content on a sandy beach?

Tidal oscillations in the water table below the beach cause significant changes in surface moisture content. On a semi-diurnal tidal timescale, these changes are especially due to submersion of the beach during high water and drainage to the water table afterwards. On a spring-neap tidal timescale, variations in overheight and hence moisture content might cause a spring-neap tidal variation in aeolian sand transport, assuming similar wind conditions.

References

Abarca E, Karam H, Hemond HF, Harvey CF. 2013. Transient groundwater dynamics in a coastal aquifer: The effects of tides, the lunar cycle, and the beach profile. *Water Resources Research* **49:** 2473–2488. doi:10.1002/wrcr.20075

Ataie-Ashtiani B, Volker RE, Lockington DA. 2001. Tidal effects on groundwater dynamics in unconfined aquifers. *Hydrological processes* **15:** 655-669.

Atherton RJ, Baird AJ, Wiggs GFS. 2001. Inter-tidal dynamics of surface moisture content on a meso-tidal beach. *Journal of Coastal Research* **17(2):** 482-489.

Baird AJ, Horn DP. 1996. Monitoring and modelling ground water behaviour in sandy beaches. *Journal of Coastal Research* **12(3):** 630–640.

Bauer BO, Davidson-Arnott RGD, Hesp PA, Namikas SL, Ollerhead J, Walker IJ. 2009. Aeolian sediment transport on a beach: Surface moisture, wind fetch and mean transport. G*eomorphology* **105**: 106-116.

Cartwright N. 2004. Groundwater dynamics and the salinity structure in sandy beaches. PhD Thesis. University of Queensland, 189 p.

Cartwright N, Nielsen P, Perrochet P. 2005. Influence of capillarity on a simple harmonic oscillating water table: Sand column experiments and modelling. *Water Resources Research* **41:** W08416. doi: 10.1029/2005WR004023.

Clarke DJ, Eliot IG. 1983. Mean sea-level and beach-width variation at Scarborough, Western Australia. *Marine Geology* **51:** 251–267.

Darke I, McKenna Neuman C. 2008. Field study of beach water content as a guide to wind erosion potential. *Journal of Coastal Research* **24(5)**: 1200-1208.

Davidson-Arnott RGD, Yang Y, Ollerhead J, Hesp PA, Walker J. 2007. The effects of surface moisture on aeolian sediment transport threshold and mass flux on a beach. *Earth surface processes and Landforms* **DOI:** 10.1002/esp1527

Emery KO, Gale JF. 1951. Swash and swash mark. *Transactions of the American Geophysical Union* **32:** 31– 36.

Gaskin GJ, Miller JD. 1996. Measurement of soil water content using a simplified impedance measuring technique. *Journal of Agricultural Engineering Research* **63**: 153-160.

Gillham RW. 1984. The capillary fringe and its effect on water-table response. *Journal of Hydrology* **67:** 307-324.

Gourlay MR. 1992. Wave set-up, wave run-up and beach water table: Interactions between surf zone hydraulics and groundwater hydraulics. *Coastal Engineering* **17:** 93-144.

Guo HP, Jiao JJ, Weeks EP. 2008. Rain-induced subsurface airflow and Lisse effect. *Water Resources Research* **44(7):** W07409. doi: 10.1029/2007WR006294

Hanslow DJ, Nielsen P. 1993. Shoreline Setup on Natural Beaches. *Journal of Coastal Research, Special Issue* **15:** 1-10.

Hegge BJ, Masselink G. 1991. Groundwater-table responses to wave run-up: an experimental study from Western Australia. *Journal of Coastal Research* **7(3):** 623– 634.

Hendriks MR. 2010. Introduction to Physical Hydrology. New York: Oxford University Press. 331 p.

Horn DP. 2002. Beach groundwater dynamics. *Geomorphology* **48:** 121-146.

Hotta S, Kubota S, Katori S, Horikawa K. 1984. Sand transport by wind on a wet sand surface. Proceedings of the 19th Coastal Engineering Conference. *American Society of Civil Engineers, New York, pp 1265-1281.*

Janssen H, Carmeliet J, Hens H. 2004. The influence of soil moisture transfer on building heat loss via the ground. *Building and environment* **39(7):** 825-836.

Khaled IM, Tsuyoshi M, Kohei N, Taku N, Hiromi I. 2011. Experimental and Modeling Investigation of Shallow Water Table Fluctuations in Relation to Reverse Wieringermeer Effect. *Open journal of soil science* **1:** 17-24. **DOI**:10.4236/ojss.2011.12003

Laycock JW. 1978. North Stradbroke Island. *Papers, Department of Geology, University of Queensland* **8(2)**: 89-96.

Lewandowski A, Zeidler RB. 1978. Beach ground-water oscillations. *Proceedings of the 16th Conference on Coastal Engineering,* pp. 2051– 2065.

Li L, Barry DA, Parlange JY, Pattiaratchi CB. 1997. Beach water table fluctuations due to wave run-up: Capillarity effects. *Water Resources Research* **33(5):** 935-945.

Li L, Barry DA, Stagnitti F, Parlange JY. 2000a. Groundwater waves in a coastal aquifer: A new governing equation including vertical effects and capillarity. *Water resources research* **36(2):** 411-420.

Li L, Barry DA, Stagnitti F, Parlange JY, Jeng DS. 2000b. Beach water table fluctuations due to spring-neap tides: moving boundary effects. *Advances in water resources* **23:** 817-824.

Liu Y, Shang S, Mao X. 2012. Tidal effects on groundwater dynamics in coastal aquifer under different beach slopes. *Journal of hydrodynamics* **24(1):** 97-106. **DOI**: 10.1016/S1001-6058(11)60223-0

Mao X, Enot P, Barry DA, Li L, Binley A, Jeng DS. 2006. Tidal influence on behaviour of a coastal aquifer adjacent to a low-relief estuary. *Journal of hydrology* **327:** 110-127.

Miyazaki T, Ibrahimi MK, Nishimura T. 2012. Shallow Groundwater Dynamics Controlled by Lisse and Reverse Wieringermeer Effects. *Journal of Sustainable Watershed Science & Management* **1 (2):** 36–45. doi: 10.5147/jswsm.2012.0065

Namikas SL, Edwards BL, Bitton MCA, Booth JL, Zhu Y. 2010. Temporal and spatial variabilities in the surface moisture content of a fine-grained beach. *Geomorphology* **114**: 303-310.

Nield JM, Wiggs GF, Squirrell RS. 2011. Aeolian sand strip mobility and protodune development on a drying beach: examining surface moisture and surface roughness patterns measured by terrestrial laser scanning. *Earth Surface Processes and Landforms* **36**: 513-522.

Nielsen P. 1990. Tidal dynamics of the water table in beaches. *Water resources research* **26(9):** 2127-2134.

Oblinger A, Anthony EJ. 2008. Surface moisture variations on a multibarred macrotidal beach: implications for aeolian sand transport. *Journal of Coastal Research* **24**: 1194-1199.

Oosterbaan RJ, Nijland HJ. 1994. Determining the saturated hydraulic conductivity. In: Drainage Principles and Applications. Ritzema HP (ed.). Wageningen, The Netherlands: *International Institute for Land Reclamation and Improvement (ILRI), Publication 16, second revised edition*, ISBN 90 70754 3 39. Pp. 435-475.

Pastoors MJH. 1992. Landelijk grondwatermodel; conceptuele modelbeschrijving RIVM november 1992.

Pollock LW, Hummon WD. 1971. Cyclic changes in interstitial water content, atmospheric exposure, and temperature in a marine beach. *Limnology and Oceanography* **16(3):** 522-535. doi: 10.4319/lo.1971.16.3.0522

Philip JR. 1973. Periodic nonlinear diffusion: an integral relation and its physical consequences. *Australian Journal of Physics* **26:** 513-519.

Raubenheimer B, Guza RT, Elgar S. 1999. Tidal water table fluctuations in a sandy ocean beach. *Water resources research* **35(8):** 2313-2320.

Roelsma J, Kselik RAL, de Vos JA. 2008. Watersysteemverkenning Noordelijke Friese Wouden. Wageningen, Alterra, Alterra-rapport 1464. 52 pp.

Schmutz PP, Namikas SL. 2011. Utility of the Delta-T Theta Probe for Obtaining Surface Moisture Measurements from Beaches. *Journal of Coastal Research* **27**: 478-484.

Schmutz PP, Namikas SL. 2013. Measurement and modeling of moisture content above an oscillating water table: implications for beach surface moisture dynamics. *Earth Surface Processes and Landforms* doi: 10.1002/esp.3418

Schmutz PP. 2014. Investigation of factors controlling the dynamics of beach surface moisture content. PhD Thesis. Louisiana State University, 160 p.

Turner IL, Coates BP, Acworth RI. 1996. The effects of tides and waves on water-table elevations in coastal zones. *Hydrogeology Journal* **4(2):** 51–69.

Turner IL, Coates BP, Acworth RI. 1997. Tides, waves and the super-elevation of groundwater at the coast. *Journal of Coastal Research* **13(1)**: 46-60.

Turner IL, Nielsen P. 1997. Rapid watertable fluctuations within the beachface: implications for swash zone sediment mobility? *Coastal Engineering* **32:** 45– 59.

Yang H, Rahardjo H, Leong E, Fredlund DG. 2004. Factors affecting drying and wetting soil-water characteristic curves of sandy soils. *Canadian Geotechnical Journal* **41:** 908–920.

Yang Y, Davidson-Arnott RGD. 2005. Rapid measurement of surface moisture content on a beach. *Journal of Coastal Research* **21**: 447-452.

Web sites

www2.nau.edu/~doetqp-p/courses/env302/lec18/LEC18.html, accessed on 20 June 2014

Appendix A

All coordinates in this appendix were measured with an RTK-GPS device, in the RD 2008 coordinate system.

A.1 Coordinates and data of the dipwells from 15-29 September

The locations of all dipwells are given in Table A.1. Measurements of groundwater levels were done manually, so apart from the bed level (Table A.2), the top of the dipwells are also given (as GW_OP, Table A.3). The values of GW_OP were not determined every day, for instance when the dipwell was submerged or due to problems with the RTK-GPS equipment. For the calculations in this thesis, the averages of GW_OP were used.

Table A-1. Coordinates of the dipwells from 15-29 September

Dipwell	x-coordinate	y-coordinate
GW1	72053.7	451873.7
GW2	72066.0	451868.1
GW3	72079.7	451862.9
GW4	72093.0	451857.3
GW5	72103.6	451852.4
GW6	72108.9	451850.6
GW7	72115.0	451847.8
GW8	72125.5	451843.5

Table A-2. Bed level heights (m) for all dipwells

Dipwell	18-sep	19-sep	20-sep	21-sep	22-sep	23-sep	24-sep	27-sep	28-sep	29-sep
GW1	-0.041	-0.100	-0.187					-0.128	0.062	0.027
GW2	0.518	0.735	0.670		0.083		0.496	0.238	0.571	0.570
GW3	0.095	0.134	0.133		0.401	0.325	0.289	0.398	0.417	0.591
GW4	0.370	0.400	0.390		0.383	0.432	0.370	0.347	0.367	0.382
GW5	1.129	1.180	1.173	1.121	1.080	0.963	0.998	0.900	0.880	0.825
GW6	1.268	1.308	1.284	1.347	1.329	1.202	1.204	1.263	1.342	1.427
GW7	1.605		1.622	1.623	1.601	1.511	1.520	1.566	1.597	1.657
GW8	2.030		2.030	2.015	2.028	2.039	2.050	2.035	2.075	2.068

Table A-3. Height of the top of the dipwells (GW_OP, in m) for all dipwells

GW_OP	17-sep	18-sep	19-sep	21-sep	21-sep	23-sep	24-sep	27-sep	28-sep	mean
GW1	0,912	0,891	0,923					0,9110	0,9450	**0,9164**
GW2	1,293	1,254			1,333		1,286	1,2740	1,2980	**1,289667**
GW3	0,881	0,846	0,878		0,925	0,896	0,866	0,8430	0,8830	**0,87725**
GW4	1,275	1,242	1,28		1,335	1,297	1,276	1,2590	1,2960	**1,2825**
GW5	1,549	1,583	1,615	1,618	1,670	1,631	1,605	1,6010	1,6280	**1,611111**
GW6	1,765	1,745	1,771	1,795	1,827	1,787	1,774	1,7700	1,7850	**1,779889**
GW7	1,891	1,882		1,942	1,949	1,934	1,925	1,9140	1,9330	**1,92125**
GW8	2,236	2,259		2,293	2,300	2,291	2,292	2,2680	2,2910	**2,27875**

A.2 Coordinates and data of the dipwells from 11 to 23 October

Before the deployment of the Keller sensors, the filters at the bottom of the dipwells were replaced. Therefore, the x- and y-coordinates of the dipwells have also changed. Their new values are given in Table A-4. The bed level next to the dipwells is given in Table A-5, and Table A-6 gives the distance from the top of the dipwell to the bed surface. Missing data are due to submerged dipwells.

To find the actual height of each sensor with respect to NAP, the distance from the top (cap) of the dipwell to the bottom of the sensor is needed. This is given in Table A-7, together with the actual sensor number and its offset in mBar.

Table A-4. X and y coordinates of the dipwells from 11 to 23 October

Dipwell	x-coordinate	y-coordinate
GW1	72063.7	451871.4
GW2	72074.5	451865.9
GW3	72085.1	451861.8
GW4	72094.5	451858.2
GW5	72101.9	451855.2
GW6	72111.5	451851.5
GW7	72118.2	451849.3
GW8	72126.9	451846.4

Table A-5. Bed level heights (m) for all dipwells

Dipwell	11-oct	12-oct	13-oct	14-oct	15-oct	16-oct	18-oct	19-oct	20-oct	23oct
GW1	-0.144	-0.015	-0.011	-0.033	-0.046	-0.022	-0.029	-0.044	-0.239	-0.035
GW2	0.263	0.246	0.427	0.37	0.304	0.318	0.361	0.346	0.132	0.127
GW3	0.582	0.608	0.653	0.585	0.556	0.566	0.646	0.620	0.510	0.392
GW4	0.761	0.794	0.852	0.789	0.761	0.770	0.756	0.725	0.767	0.657
GW5	0.786	0.821	0.879	0.967	0.982	1.008	1.013	0.995	1.016	0.891
GW6	1.393	1.459	1.466	1.453	1.454	1.469	1.466	1.445	1.416	
GW7	1.683	1.730	1.798	1.724	1.747	1.755	1.737	1.726	1.711	1.401
GW8	2.090	2.114	2.161	2.116	2.126	2.129	2.113	2.084	2.082	1.709

Table A-6. Distance from the top of the dipwell to the bed surface (m) for all dipwells

Dipwell	11-oct	12-oct	13-oct	14-oct	15-oct	16-oct	18-oct	19-oct	20-oct	23oct
GW1	1.02	0.9	0.91	0.91	0.915	0.9	0.99	0.915		0.905
GW2	0.6	0.61	0.5	0.52	0.565	0.56	0.515	0.49		0.72
GW3	0.54	0.53	0.52	0.565	0.585	0.585	0.495	0.5		0.745
GW4	0.41	0.4	0.4	0.53	0.43	0.44	0.44	0.445	0.43	0.53
GW5	1	1	1	0.86	0.83	0.83	0.815	0.83	0.81	0.935
GW6	1.42	1.39	1.4	1.39	1.395	1.395	1.345	1.385	1.435	
GW7	1.38	1.37	1.37	1.37	1.36	1.36	1.335	1.375	1.345	2
GW8	1.53	1.55	1.55	1.53	1.54	1.54	1.505	1.57	1.58	1.98

Table A-7. Deployment data for the dipwells

Dipwell	sensor number	cap to bottom sensor (m)	Bottom sensor to actual sensor (m)	offset (mBar)
GW1	13969	1.865	0.02	-0.5
GW2	13967	1.92	0.02	31
GW3	13731	1.93	0.02	24.8
GW4	13736	1.885	0.02	-1.2
GW5	13965	3.37	0.02	-0.1
GW6	13732	3.36	0.02	2.8
GW7	13966	3.365	0.02	40.8
GW8	13968	3.375	0.02	8.3

A.3 Other coordinates

Coordinates of pressure transducer OSSI1

Date	x-coordinate	y-coordinate	Bed level (m NAP)
17 sep	72037.579	451877.722	-1.135
18 sep	72037.401	451877.499	-1.113
20 sep	72037.489	451877.444	-1.202
23 sep	72037.561	451877.442	-0.666
26 sep	72037.545	451877.233	-0.780
27 sep	72037.680	451877.407	-0.876
28 sep	72037.577	451877.459	-1.128
30 sep	72037.646	451877.485	-1.045
01 oct	72037.695	451877.441	-1.140
02 oct	72037.524	451877.365	-1.129
04 oct	72037.675	451877.583	-1.296
06 oct	72037.572	451877.533	-1.180
15 oct	72037.601	451877.589	-1.117
19 oct	72037.559	451877.496	-1.058
23 oct	72037.692	451877.834	-0.817

Coordinates of the borehole and dipwell with the deep filter of S. Huizer

X	72250.22
Y	451819.17
Z	4.3

Appendix B. Time series of groundwater levels

Figures B1-B7 give the groundwater signals as recorded by the Keller sensors in GW2-GW8, respectively. High and low water levels are also indicated. In all figures, time is in days, starting with t=0 at October 8.

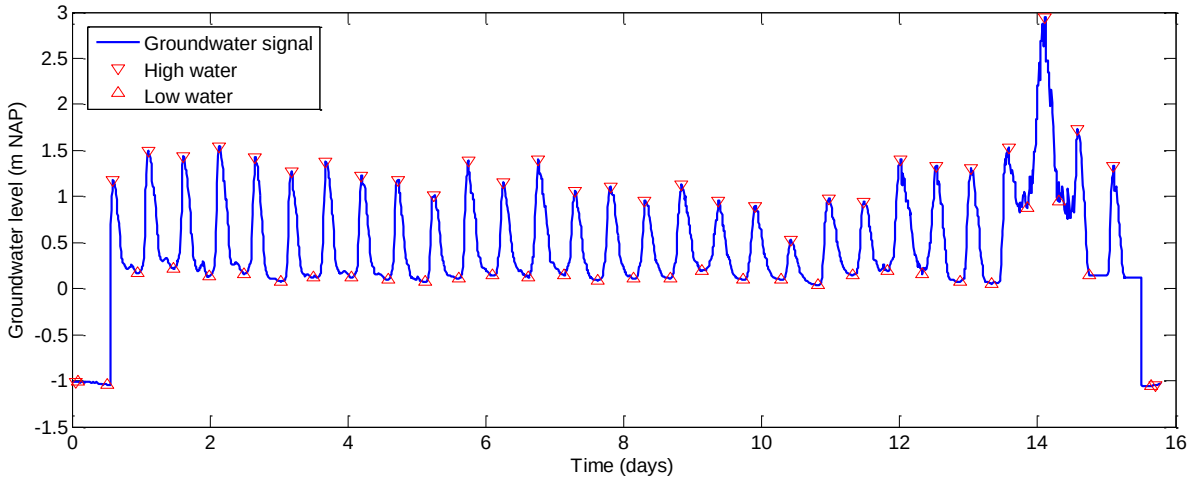

Figure B-1. Groundwater level in GW2

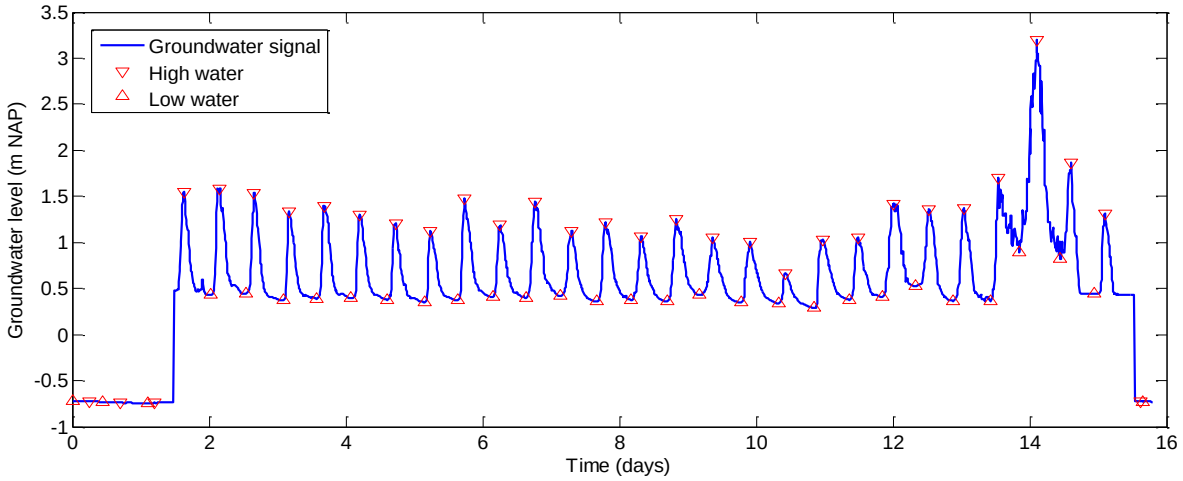

Figure B-2. Groundwater level in GW3

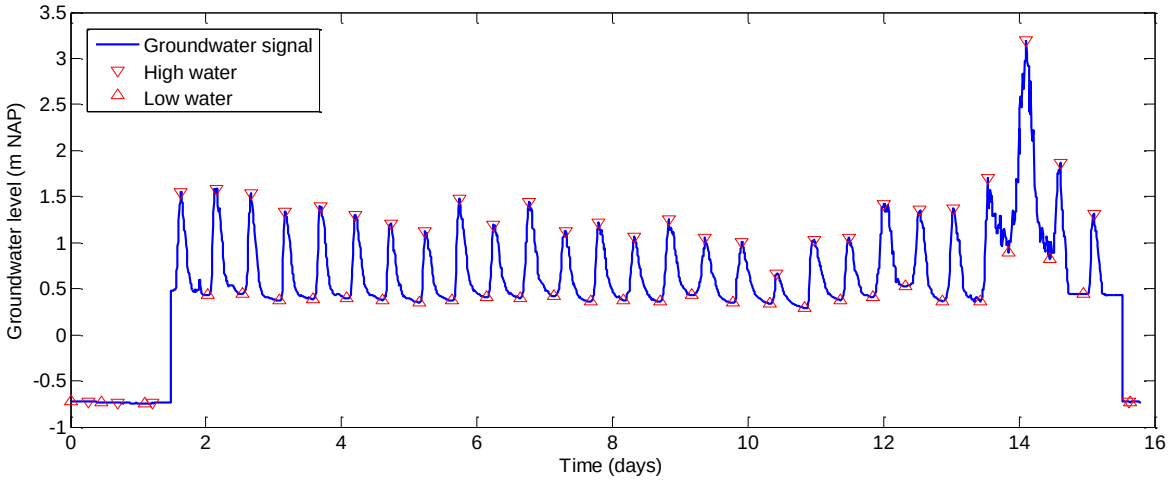

Figure B-3. Groundwater level in GW4

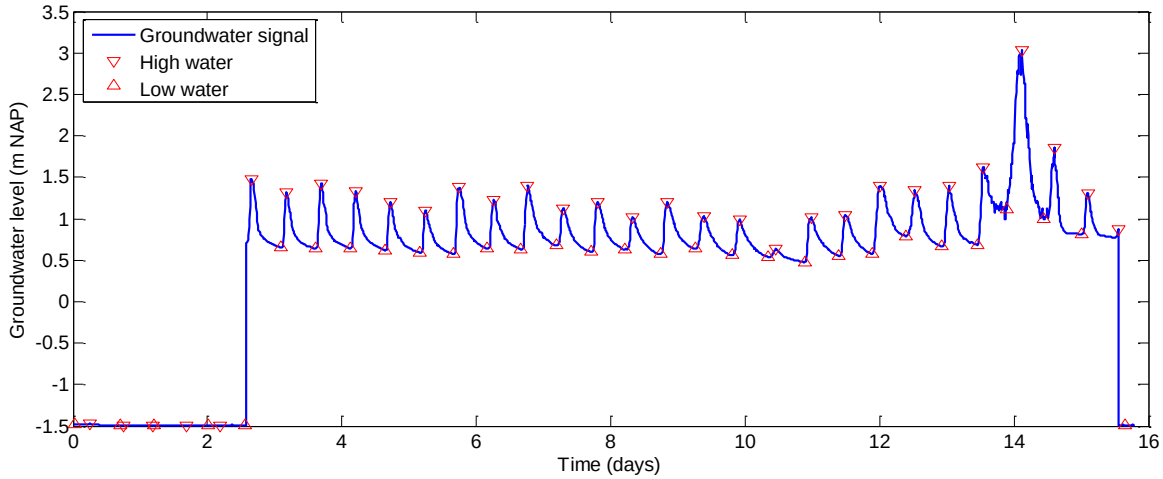

Figure B-4. Groundwater level in GW5

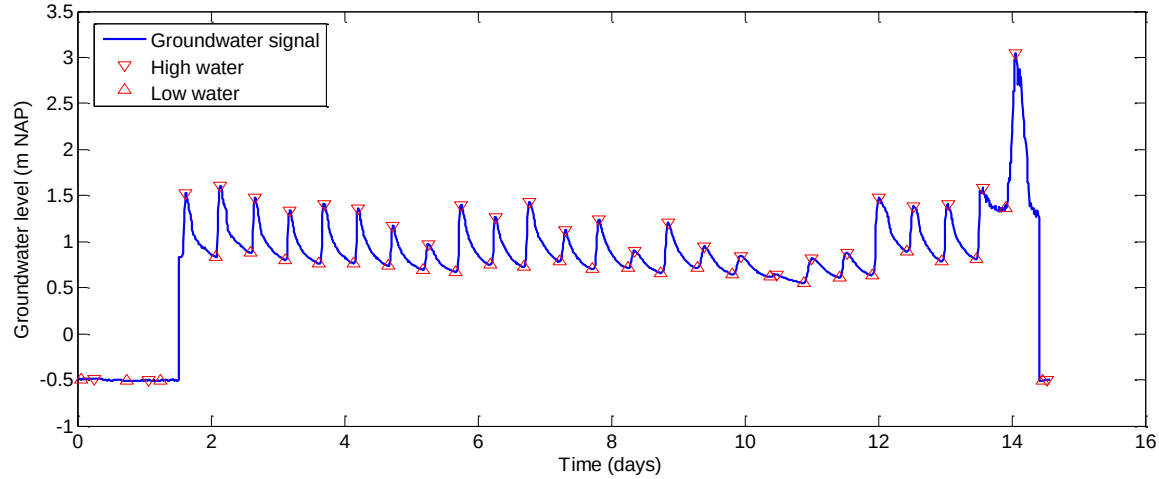

Figure B-5. Groundwater level in GW6

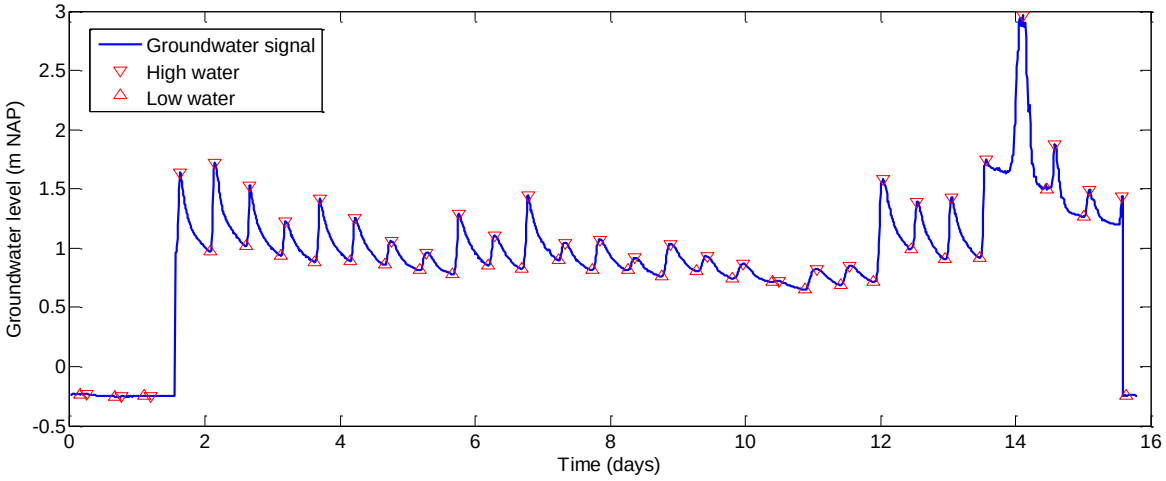

Figure B-6. Groundwater level in GW7

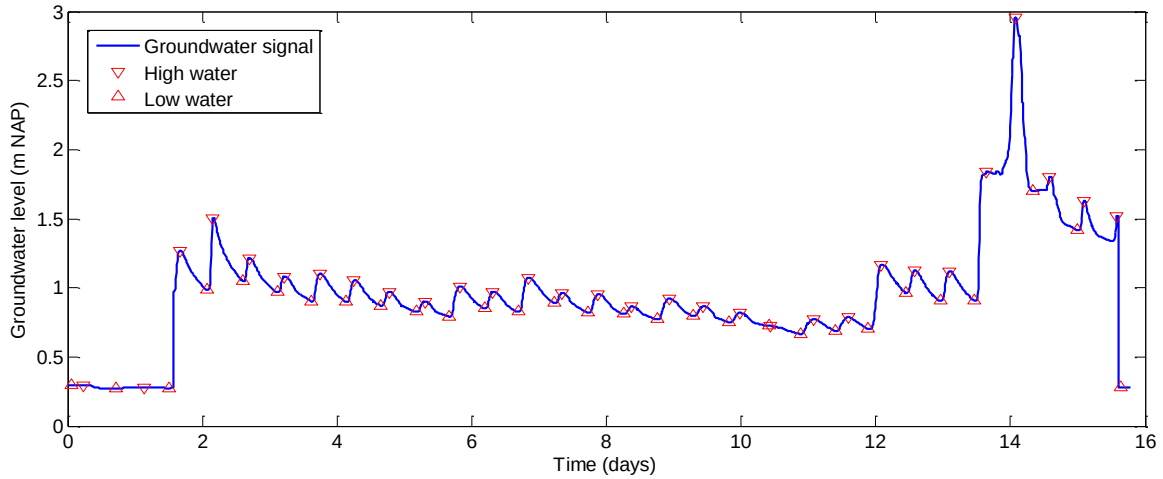

Figure B-7. Groundwater level in GW8